3-14-2014

Thermal Characterization of the Air Force Institute of Technology Solar Simulation Thermal Vacuum Chamber

Daniel M. Hatzung

THERMAL CHARACTERIZATION OF THE AIR FORCE INSTITUTE OF TECHNOLOGY SOLAR SIMULATION THERMAL VACUUM CHAMBER

THESIS

Daniel M. Hatzung, Captain, USAF

AFIT-ENY-14-M-23

DEPARTMENT OF THE AIR FORCE
AIR UNIVERSITY

AIR FORCE INSTITUTE OF TECHNOLOGY

Wright-Patterson Air Force Base, Ohio

The views expressed in this thesis are those of the author and do not reflect the official policy or position of the United States Air Force, Department of Defense, or the United States Government.

AFIT-ENY-14-M-23

THERMAL CHARACTERIZATION OF THE AIR FORCE INSTITUTE OF TECHNOLOGY SOLAR SIMULATION THERMAL VACUUM CHAMBER

THESIS

Presented to the Faculty

Department of Aeronautical and Astronautical Engineering

Graduate School of Engineering and Management

Air Force Institute of Technology

Air University

Air Education and Training Command

In Partial Fulfillment of the Requirements for the

Degree of Master of Science in Astronautical Engineering

Daniel M. Hatzung, BS

Captain, USAF

March 2014

AFIT-ENY-14-M-23

THERMAL CHARACTERIZATION OF THE AIR FORCE INSTITUTE OF TECHNOLOGY SOLAR SIMULATION THERMAL VACUUM CHAMBER

Daniel M. Hatzung, BS
Captain, USAF

Approved:

// Signed //	13 Mar 14
Maj James L. Rutledge, PhD (Chairman)	Date
// Signed //	14 Mar 14
Eric D. Swenson, PhD (Member)	Date
// Signed //	14 Mar 14
Richard G. Cobb, PhD (Member)	Date

Abstract

Although predictive thermal modeling on CubeSats has previously been accomplished, a method to validate these predictive models with terrestrial experiments is essential for developing confidence in the model. As a part of this effort, AFIT has acquired a new Solar Simulation Thermal Vacuum Chamber. This research analyzed the thermal environment to which a test article is exposed within the AFIT Solar Simulation Thermal Vacuum Chamber. A computational model of the thermal environment in the chamber was created and then validated using an experimental buildup approach through thermal balance testing of the empty chamber and an aluminum plate. First, the modeled surface temperatures of the thermal vacuum chamber interior walls were validated within $T_{error} < 4°C$ of steady-state experimental data. Next, the aluminum plate computational model was validated within $T_{error} < 1°C$ of steady-state experimental data. Through these results, this research provides the capability to validate spacecraft and payload computational thermal models within the thermal vacuum chamber environment by comparing computational predictions to experimental data for steady-state cases. Additionally, this research validated an upgrade to increase optical performance of the TVAC by bolting a copper plate coated with Aeroglaze® black paint to the top of the platen, ensured safe procedures are in place for solar simulation, and improved the temperature controller performance.

For my amazing wife and darling daughters

Acknowledgments

I am extremely grateful for many people's contributions to my thesis. Thank you to my thesis advisor, Major Rutledge, for his continual guidance, insight, and encouragement throughout this research. I am also grateful for the help of Mr. Chris Sheffield and his consistent and copious efforts to ensure I had functional test equipment as often as possible, along with his assistance in setting up and taking down experiments. Thank you, Dr. Cobb and Dr. Swenson for serving on my committee and providing me many opportunities for enrichment while I've been at AFIT. Thank you also to all of the Astro students who aided me in setting up and taking down TVAC experiments at extremely odd hours. Lastly, thank you most of all to my wife for her continual support of my career and to my daughters for sacrificing time with their dad in order for me to accomplish this.

Daniel M. Hatzung

Table of Contents

List of Figures

Page

Page

List of Tables

Page

List of Acronyms

AFIT	Air Force Institute of Technology
CONOPS	Concept of Operations
CSRA	Center for Space Research and Assurance
DoD	Department of Defense
GEVS	General Environmental Verification Standards
IR	Infrared
JSpOC	Joint Space Operations Center
MSFC	Marshall Space Flight Center
NASA	National Aeronautics and Space Administration
NPS	Naval Postgraduate School
NPS-SCAT	Naval Postgraduate School Solar Cell Array Tester
PID	Proportional Integral Derivative
RTD	Resistance Temperature Detector
TVAC	Thermal Vacuum Chamber

List of Symbols

A	area, m^2
$A_{reflected}$	incident surface area of the spacecraft in line of sight of solar radiation reflected off the Earth, m^2
A_s	area of the surface, m^2
A_{solar}	the incident area of the spacecraft in line of sight of direct solar radiation, m^2
c	speed of light in vacuum, 2.998×10^8 m/s
c_p	specific heat at constant pressure, J/kg•K
erf	Gaussian error function
$E_{\lambda,b}$	spectral emissive power of a blackbody, W/m^2•μm
$\dot{E}_g$	rate of energy generation, W
$\dot{E}_{in}$	rate of energy transfer into a control volume, W
$\dot{E}_{out}$	rate of energy transfer out of a control volume, W
$\dot{E}_{st}$	rate of increase of energy storage within a control volume, W
G	incident radiation heat flux hitting surface, W/m^2
h	convection heat transfer coefficient, W/m^2•K; Planck constant, 6.626×10^{-34} J•s
IR_{Earth}	Earth-emitted infrared heat flux, W/m^2
k	thermal conductivity, W/m•K; Boltzmann constant, 1.381×10^{-23} J/K
K_P	proportional control coefficient
K_I	integral control coefficient
K_D	derivative control coefficient
m	mass, kg
P	pressure, Torr
q	heat rate, W
q_{solar}	combined direct and albedo solar heat rate absorbed by a spacecraft, W
$\dot{q}$	rate of energy generation per unit, W/m^3
$\vec{q}''$	heat flux, W/m^2
R	albedo value
S	direct solar heat flux, W/m^2
t	time, s
T	temperature, K
T_{bottom}	temperature of the bottom surface, K
T_{error}	difference between computationally predicted and measured temperatures, K
T_{fluc}	temperature fluctuation amplitude, K
T_i	initial temperature at all locations within the material, K
T_s	surface temperature, K
T_∞	fluid temperature, K
x	depth through the material from the bottom surface, m
α	absorptivity; thermal diffusivity, m^2/s
ε	emissivity
λ	wavelength, μm
ρ	density, kg/m^3; reflectivity
σ	Stephan-Boltzmann constant, 5.67×10^{-8} W/m^2•K^4
τ	transmissivity

THERMAL CHARACTERIZATION OF THE AIR FORCE INSTITUTE OF TECHNOLOGY SOLAR SIMULATION THERMAL VACUUM CHAMBER

I. Introduction

Motivation

The CubeSat class of nanosatellites continues to become a preferred choice for Department of Defense (DoD) and university research satellites. A CubeSat is specifically defined as a nanosatellite made of a combination of one to six approximately 10x10x11 cm cubes [1]. While CubeSats have proven to be a cost effective configuration for research satellites, a mission failure rate of 30% and an average on-orbit life of less than 200 days demonstrate issues with survivability through launch and in the space environment [2]. Inadequate thermal design, analysis and testing are factors contributing to mission failures and shortened on-orbit life [2].

The Air Force Institute of Technology (AFIT) Center for Space Research and Assurance (CSRA) recently acquired a solar simulation thermal vacuum chamber (TVAC) sized specifically for CubeSats and small payloads in order to increase its thermal analysis validation and test capabilities. The system is capable of reaching high vacuum pressures, defined as 10^{-9} Torr < P< 10^{-3} Torr, while controlling the temperature of the chamber environment [3]. The solar simulator is a lamp radiating one-sun equivalent collimated light into the chamber to simulate solar heat flux in a vacuum environment. A picture of the chamber is shown in Figure 1. As with any custom designed piece of hardware, it is important to do thorough testing in order to understand the full capabilities of the equipment and develop methods of ideal use. This research

provides a framework for ideal use of the chamber along with recommendations for improvements.

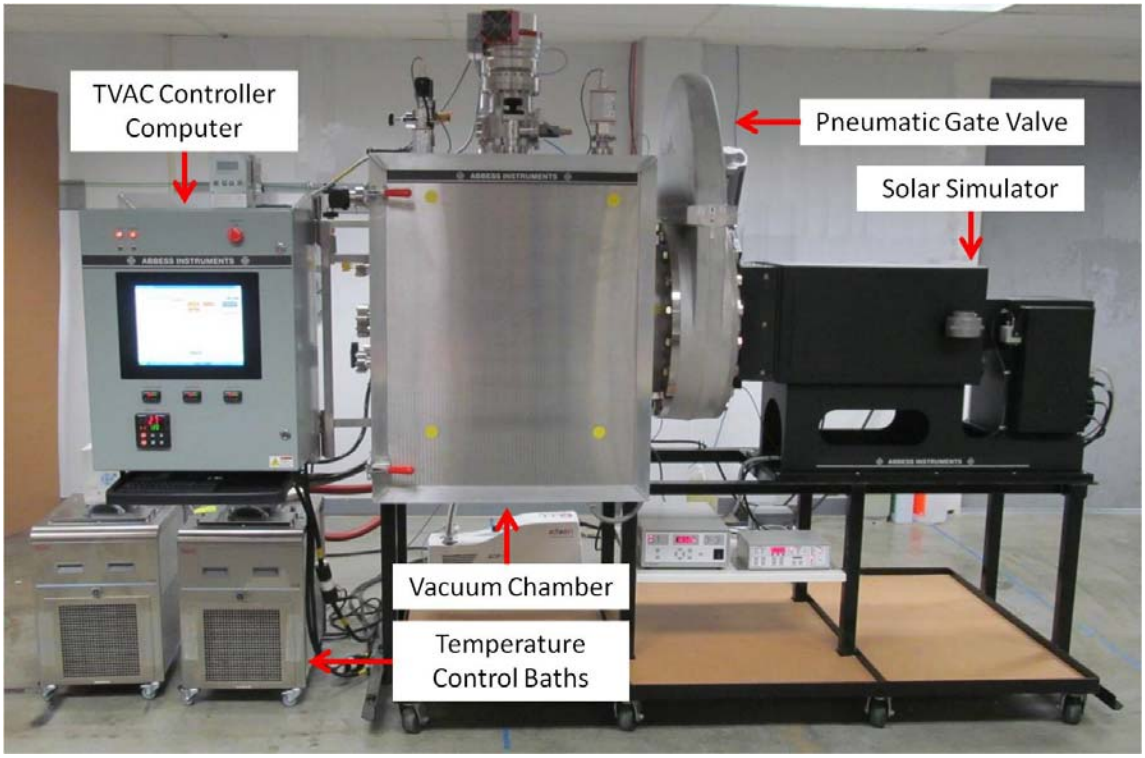

Figure 1 AFIT Solar Simulation TVAC

Another facet of increasing CubeSat and small payload thermal capabilities is to improve thermal analysis and validation techniques. The most rigorous example of thermal analysis practice for CubeSats found is to develop a predictive computational thermal model for a cold and hot worst-case scenario based on first-order predictions of the on-orbit thermal environment and planned internal heat generation [4]. This determines the predicted spacecraft temperature envelope. The spacecraft is then tested in a thermal vacuum chamber, and the temperature of the chamber is configured to simulate the worst-case predicted on-orbit thermal environment in order to verify

survivability. While this analysis process provides a framework for thermal design considerations and component selection, the spacecraft predictive computational thermal model is not typically validated to provide confidence in on-orbit temperature predictions.

A validated computational thermal model of the TVAC used for environmental testing would provide a validation tool for spacecraft predictive thermal models. Simulations of the spacecraft thermal model would be run within the TVAC environment computational thermal model and compared to a thermal balance test, a test in which the spacecraft hardware is tested to steady-state at hot and cold worst-case scenarios, accomplished in the same TVAC as was modeled. The resulting data would provide confidence in the relative accuracy of a predictive model or the necessary feedback in order to modify it. More specifically, a thermal model had not previously been developed and validated for the AFIT Solar Simulation TVAC. This research works to provide this computational model validation capability for AFIT.

Thesis Objectives

The goal of this research is analyze and characterize the thermal environment within AFIT's Solar Simulation TVAC. Primarily, this research entails conducting experiments to characterize the performance capabilities of the TVAC and develop a computational thermal model of the TVAC environment using Thermal Desktop® for use by future AFIT students or staff. The TVAC computational thermal model could then be used to compare their computational thermal models to experimental TVAC thermal balance test data for validation. The TVAC environment thermal computational model

will be validated through a series of experiments with a build-up approach developed to sequentially increase complexity. Also, this research will validate an upgrade to increase optical performance of the TVAC by bolting a copper plate coated with Aeroglaze® black paint to the top of the platen, validate and improve the temperature controller performance, and ensure appropriate practices are in place for solar simulation.

Thesis Overview

Chapter 2 discusses the physical and mathematical concepts and published work pertaining to this research. Then Chapter 3 provides an overview of the computational and experimental methodology of this research. This is followed by the computational and experimental results and analysis in Chapter 4. Lastly, Chapter 5 discusses the conclusions of this research along with recommendations for future work.

II. Literature Review

Chapter Overview

This chapter provides a summary of the mathematical and physical concepts and terminology incorporated into this research. Specifically, this chapter provides an overview of the modes of heat transfer relevant to this research, along with how those modes are incorporated into a computational method of spacecraft thermal analysis. Also, TVAC testing purposes and methods are discussed, along with an overview of Proportional Integral Derivative (PID) control, the type of control method used for temperature control within the AFIT Solar Simulation TVAC. Lastly, this chapter reviews published spacecraft test and analysis research pertaining to this research.

Conduction

Thermal conduction is the transport of energy through a medium via random atomic or molecular activity [5]. Conduction heat transfer occurs when particles collide and higher temperature, and therefore more energetic, particles transfer energy to lower temperature, less energetic particles. Because of this, conduction always transfers energy in the direction of decreasing temperature. Conduction is typically described as diffusion of energy due to random molecular motion or by lattice waves induced by atomic motion. Conduction occurs within gases, liquids, or solids and is multi-dimensional.

Conduction Terminology and Defining Equations

There are several thermophysical properties of materials critical to a material's ability to conduct effectively [5]. The most prominent of these properties is thermal

conductivity, k. Thermal conductivity is considered a transport property as it is a measure of the rate at which energy is transported by diffusion. More specifically, thermal conductivity establishes a linear relationship between the heat flux and the temperature gradient as shown in Fourier's law in Equation 1:

$$q_x = -kA\frac{dT}{dx} \tag{1}$$

where q_x is the heat rate in the x-direction (W), k is the thermal conductivity (W/m•K), A is the cross-sectional area of the material (m^2), and T is the temperature (K).

In this simplified format of Fourier's law, conduction is assumed to be uniform and one-dimensional. Since the heat rate increases linearly with increasing thermal conductivity, Equation 1 demonstrates how the thermal conductivity determines the effectiveness of conduction heat transfer through the material. The greater the thermal conductivity of a material, the more effectively the material will transfer thermal energy [5]. On the contrary, the lower the thermal conductivity of a material, the more effective an insulator the material is. Generalizing Fourier's law to be a multi-dimensional vector quantity results in the heat flux per unit area in Equation 2:

$$\vec{q}'' = -k\nabla T = -k\left(\boldsymbol{i}\frac{\partial T}{\partial x} + \boldsymbol{j}\frac{\partial T}{\partial y} + \boldsymbol{k}\frac{\partial T}{\partial z}\right) \tag{2}$$

where q'' is the heat flux (W/m^2).

Factoring only conduction into a rate version of the conservation of energy equation for a differential control volume results in the heat diffusion equation:

$$\frac{\partial}{\partial x}\left(k\frac{\partial T}{\partial x}\right) + \frac{\partial}{\partial y}\left(k\frac{\partial T}{\partial y}\right) + \frac{\partial}{\partial z}\left(k\frac{\partial T}{\partial z}\right) + \dot{q} = \rho c_p\frac{\partial T}{\partial t} \tag{3}$$

where $\dot{q}$ is the rate of energy generation per unit volume (W/m^3), ρ is the material density (kg/m^3), c_p is the material specific heat at constant pressure (J/kg•K), and t is time (s).

Two important properties shown in Equation 3 are critical to conduction heat transfer analysis, density and specific heat at constant pressure, c_p [5]. The product of these two properties is the volumetric heat capacity, ρc_p, which is a measure of the material's thermal energy storage capability. As long as thermal conductivity is constant throughout a uniform volume, k can be taken out of each of the partial derivatives and divided over to the right hand side of Equation 3 as shown in Equation 4:

$$\nabla^2 T + \frac{\dot{q}}{k} = \frac{1}{\alpha}\frac{\partial T}{\partial t} \tag{4}$$

where α is the thermal diffusivity (m^2/s) as defined in Equation 5:

$$\alpha = \frac{k}{\rho c_p} \tag{5}$$

A material with a high thermal diffusivity will react quickly to thermal changes, while low thermal diffusivity materials will take longer to reach new equilibrium states. There are also many applications in which there is no internal heat generation within a body. In these cases, the heat generation term in Equation 4 drops out. Because of this, thermal diffusivity as a combined material property becomes more important to transient conduction scenarios than thermal conductivity alone.

Since Equation 4 is a partial differential equation, it is a difficult equation to solve analytically beyond two-dimensional conduction with no heat generation. For this reason, numerical techniques such as the finite difference or finite element methods can be used in order to achieve good approximations of the temperatures and heat rates within a transient multi-dimensional problem.

Steady-State and Transient Conduction

There are two scenarios to consider when doing conduction analysis, steady-state equilibrium and transient changes to the system. Steady-state analysis is applied to scenarios where the temperature of any location within a system is not dependent on time. The time-dependence of stored energy shown in Equation 4 demonstrates that there must be no change to the amount of energy stored in the system for this to occur [5]. This then means there must be negligible net energy exchange across the system boundary and energy generation within the system must be constant. Lastly, enough time must pass for the system to reach a state of thermal equilibrium.

Transient analysis accounts for all time-dependent cases, encompassing all cases excluded from steady-state analysis as previously defined. Since the heat diffusion equation is parabolic, any perturbation to the energy rate in or out of the system, the energy generation within the system, or the energy stored in the system causes the temperature at every point within the system to begin to change [5]. The system is no longer in equilibrium and temperature fields within the system fluctuate and change.

Convection

While conduction describes a diffusion of energy throughout a medium, fluid motion also works as an energy transfer process [5]. Convection heat transfer occurs when there is a combination of energy diffusion and fluid motion. When there is a temperature gradient, these processes cause a transfer of heat from more energetic molecules to less energetic molecules. A prime example of convection is when a fluid is flowing over a higher temperature stationary surface. Over time, the molecules in the

fluid in contact with the surface absorb energy from the surface into the fluid. This energy transfer increases the temperature of the fluid while decreasing the temperature of the surface. Similar to conduction, the heat flux and the temperature gradient are linearly related by a proportionality constant, the convection heat transfer coefficient (h), as shown in Equation 6:

$$q'' = h(T_s - T_\infty) \quad \textbf{(6)}$$

where h is the convection heat transfer coefficient (W/m^2•K), T_s is the surface temperature (K), and T_∞ is the fluid temperature. The convection heat transfer coefficient is the rate constant for convection and is dependent on surface geometry, the nature of fluid motion, and thermodynamic and transport properties of the fluid [5].

Convection can be generally classified in one of two categories depending on the nature of fluid motion. Forced convection occurs when motion in the fluid is caused by external means. A fan blowing air over a circuit board is an example of forced convection. Contrarily, free (or natural) convection occurs when density differences in the fluid cause warmer and therefore less dense molecules to rise within the fluid due to buoyancy forces, and then they are replaced by the cooler and therefore more dense molecules. The rise of hot gasses through a chimney is an example of free convection.

Radiation

Thermal radiation is defined as emitted electromagnetic radiation that is detected as heat [6]. The thermal radiation portion of the electromagnetic spectrum includes a portion of the long-wavelength ultraviolet region, along with the visible, short-

wavelength infrared (IR), and long-wavelength IR regions. Thermal radiation differs most significantly from conduction and convection in two ways. Since radiation transfers heat through electromagnetic waves and photons, radiation does not need a medium in order to transfer heat from one body to another. Also, while heat transfer by conduction and convection is dependent on the temperature difference between two locations raised to the first power, radiation between two bodies is dependent on the absolute temperature of each body raised to the fourth power.

Blackbody Radiation

In order to understand the radiation properties of real surfaces, they are compared to an ideal radiating body called a blackbody. A blackbody absorbs all incident radiation in all wavelengths and directions [5]. A blackbody also emits radiation diffusely as a function of wavelength and temperature and is the most effective emitter for that given wavelength and temperature. Based on these attributes, a blackbody is considered a perfect absorber and emitter and is the ideal standard by which all other surface's properties are measured. The temperature and wavelength dependence of a blackbody is defined by the Planck distribution shown in Equation 7 [7]:

$$E_{\lambda,b}(\lambda,T) = \frac{2\pi hc^2}{\lambda^5[e^{(hc/\lambda kT)} - 1]} \tag{7}$$

where $E_{\lambda,b}$ is the spectral emissive power of a blackbody (W/m^2•μm), λ is the wavelength (μm), h is the Planck constant (6.626x10^{-34} J•s), c is the speed of light in vacuum (2.998x10^8 m/s), and k is the Boltzmann constant (1.381x10^{-23} J/K). The spectral emissive power of the Sun (T=5900 K) and an object at room temperature (T=300 K) are shown in Figure 2.

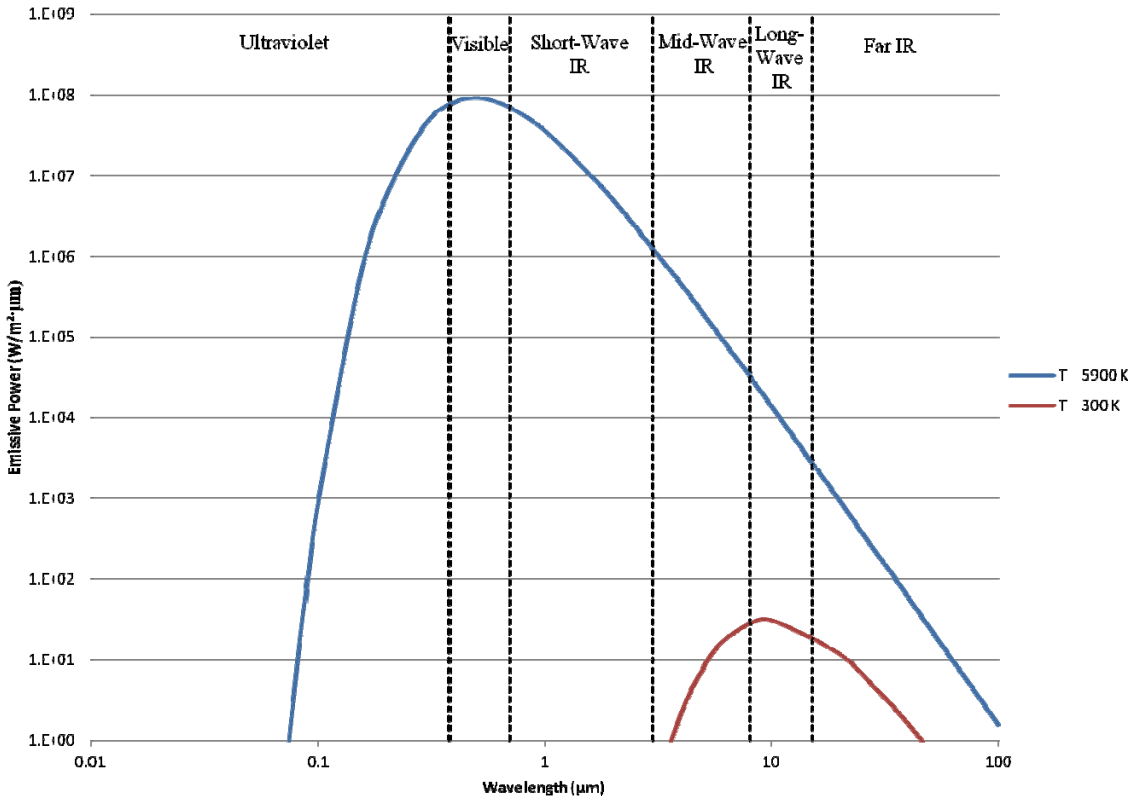

Figure 2 Blackbody Temperature-Wavelength Curve

A blackbody emits the greatest amount of radiation at the wavelength matching the peak value on the respective temperature curve. For example, the sun is a blackbody emitting at $T = 5900$ K primarily in the visible wavelengths.

Radiation Terminology and Defining Equations for Real Surfaces

The capabilities of real surfaces to absorb and emit radiation are based on four surface optical properties [5]. Emissivity (ε) is a measure of how well a surface emits radiation as compared to a blackbody. Remembering radiation emitted by a surface is a

function of temperature to the fourth power, the method of calculating the emitted heat flux is shown in Equation 8:

$$q_{out} = \varepsilon \sigma T_s{}^4 A_s \quad \textbf{(8)}$$

where q_{out} (W) is the emitted heat rate from the surface, ε is the emissivity, σ (5.67×10^{-8} W/m^2•K^4) is the Stephan-Boltzmann constant, and A_s (m^2) is the area of the surface.

Similarly, absorptivity, α, is a measure of how well a surface absorbs radiation as compared to a blackbody. This is demonstrated in Equation 9 using an arbitrary radiation source absorbed by a surface:

$$q_{in} = \alpha G A_s \quad \textbf{(9)}$$

where q_{in} (W) is the heat rate into the surface, α is the absorptivity, and G (W/m^2) is the incident radiation heat flux hitting the surface.

Emissivity and absorptivity of real surfaces vary as a function of wavelength and direction, while emissivity also varies to a relatively small degree as a function of temperature. Values for emissivity and absorptivity vary from zero to one and are based on the respective emitted or absorbed radiation by the real surface as compared to the emitted or absorbed radiation of a blackbody at the same temperature. Due to large variations in manufactured surface finishes and dependence on wavelength, direction, and temperature, values for emissivity and absorptivity can be difficult to determine and have significant uncertainty.

Since solar radiation is the dominant form of incident radiation on Earth or in Earth's orbit, published absorptivity values refer to the surface's ability to absorb solar radiation (radiation in the UV, visible, and short-wavelength IR spectrums).

Since wavelength of emitted radiation is a function of temperature of the surface as shown in Figure 2, surfaces on Earth or in Earth's orbit predominantly emit in the long-wavelength IR spectrum, similar to a blackbody at about T = 300 K. Because of this, published emissivity values refer to a surface's ability to emit radiation within that spectrum. Also, Kirchhoff's law of thermal radiation states that for a given temperature at a specific wavelength, the absorptivity and emissivity of a real surface are equal [5]. Through this understanding, published surface emissivity values are also used for surface absorptivity of long-wavelength IR radiation.

Just as with other discussions on surface optical properties, reflectivity refers to the portion, on a zero to one scale, of incident radiation reflected by the surface [5]. For an opaque surface, any radiation that is not absorbed by the surface will be reflected as shown in Equation 10:

$$\alpha + \rho = 1 \tag{10}$$

where ρ is reflectivity.

When a surface is semi-transparent, the portion of incident radiation that is not absorbed or reflected by the surface is transmitted through the surface as shown in Equation 11:

$$\alpha + \rho + \tau = 1 \tag{11}$$

where τ is transmissivity [5].

For the surface of a material, with a known mass and surface area, Equation 12 demonstrates an energy balance for the material, assuming the rest of the surfaces of the material are isothermal:

$$q_{in} - q_{out} = \dot{E}_{st} \tag{12}$$

where $\dot{E}_{st}$ (W) is the rate of change of energy stored in the body.

For a material of known volume and density, the rate of change of energy storage in the body is defined in :

$$\dot{E}_{st} = mc_p \frac{dT_s}{dt} \tag{13}$$

where m (kg) is the mass of the body.

Equations 8, 9, and 13 can then be substituted into Equation 12:

$$\alpha G A_s - \varepsilon \sigma {T_s}^4 A_s = mc_p \frac{dT_s}{dt} \tag{14}$$

As shown in Equation 14, a basic one-dimensional radiation problem is a non-linear differential equation with temperature raised to the fourth power. Once multiple bodies with multiple surfaces, multiple sources of incident radiation, and the directionality of each radiation source are all factored in, it is evident that real-world radiation problems must be solved computationally.

Heat Transfer in the Space Environment

Within the vacuum of space, radiation and conduction are the dominant methods of heat transfer. Unless a spacecraft uses cryogenic cooling systems, atmospheric compartments for manned spaceflight, or heat pipes, there are no fluids in space to enable convection to occur. In the CubeSat class of spacecraft, pressurized compartments are highly unlikely to be used due to volume and mass constraints. Heat pipes utilize evaporation of a fluid to absorb heat from a hot surface in contact with one end of the pipe and condensation at the other end of the pipe to transfer heat through the pipe to a

cold surface in contact with the pipe. While heat pipes can be used on CubeSats, convection is localized within the heat pipe interior. Without most convective cooling options, many conventional terrestrial thermal energy management options for electronics, such as fans and fins, are not viable.

Spacecraft orbiting Earth absorb three types of radiation from the space environment: direct solar radiation, albedo radiation, and Earth-emitted infrared (IR) radiation [8]. Electronic components on-board the spacecraft also radiate dissipated heat to the rest of the spacecraft due to inherent inefficiencies in powering electronics. The only means for a spacecraft to transfer any of this absorbed energy back into space is by emitting IR radiation back into deep space or to the Earth, since conduction would require the spacecraft to have surface contact with another medium. Considering the system boundary to encompass the entire spacecraft, thermal control is typically accomplished through a balance of absorbed radiation from the space environment, radiation emitted back into space, and heat generated by electrical components within the spacecraft. Conduction and internally-emitted IR radiation then combine to provide a network for heat transfer within the spacecraft.

Direct Solar Radiation

Direct solar radiation (S) is the most significant heat flux on orbit with a minimum magnitude of $S = 1322$ W/m^2 [8]. Depending on Earth's position within its orbit around the Sun, the heat flux varies from 1322 W/m^2 < S < 1414 W/m^2 with the minimum at Summer Solstice (the Earth's furthest distance from the Sun) and the maximum at Winter Solstice (the Earth's closest distance from the Sun). The solar heat flux at the Earth's mean distance from the sun is $S = 1367$ W/m^2 and is known as the solar constant. The

solar cycle does not have a significant effect on the magnitude of solar heat flux. Solar radiation is absorbed 7% in ultraviolet, 46% in visible, and 47% in short-wavelength infrared wavelengths as shown in Figure 2. Since radiation is directional and optical, the spacecraft must be in line of sight of the sun in order to absorb solar heat flux.

Albedo Radiation

Albedo radiation refers to incident solar radiation reflected back at the spacecraft off the Earth's surface [8]. Since albedo is based on reflectivity, the spacecraft only absorbs albedo radiation when solar radiation reflected off of the Earth is in line of sight of the spacecraft. Albedo radiation heat flux is generally considered as a fraction of the solar radiation heat flux. Because of the different optical properties of cloud cover, polar ice caps, land, and water, Earth's reflectivity is not uniform. In general, land mass tends to have greater reflectivity than water and because of snow and ice, greater latitudes have greater reflectivity. Albedo also tends to increase due to cloud cover and smaller solar-elevation angles. Due to the complexity and uncertainty involved, albedo values used within industry tend to vary. Depending on the complexity necessary, a constant value or latitude/longitude varying values can be used for computational modeling. Albedo values, R, measured during a National Aeronautics and Space Administration (NASA) Marshall Space Flight Center (MSFC) study varied from $0.06 < R < 0.5$ as a fraction of solar radiation heat flux in Low Earth Orbit [9]. Since albedo acts as a fraction of the solar radiation, albedo and direct solar heat flux can be substituted into Equation 9 to find combined heat flux from these two sources absorbed by the spacecraft [10]:

$$q_{solar} = \alpha S\left(A_{solar} + RA_{reflected}\right) \tag{15}$$

where q_{solar} (W) is the combined direct and albedo solar heat rate absorbed by a spacecraft, S (W/m^2) is the direct solar heat flux, A_{solar} (m^2) is the incident area of the spacecraft area in line of sight of direct solar radiation, R is the albedo value, and $A_{reflected}$ (m^2) is the incident area of the spacecraft in line of sight of solar radiation reflected off the Earth.

This method provides a conceptual understanding of how an albedo value is factored into determining the heat flux absorbed by the spacecraft; however, these environmental heat loads vary with time throughout the orbit. This calculation needs to be accomplished for every position throughout the orbit.

Earth-Emitted Infrared Radiation

The solar radiation heat flux absorbed and not reflected by the Earth is eventually emitted by the Earth as long-wavelength infrared radiation [8]. In general, warmer areas of the Earth emit IR radiation at a greater magnitude, which is due to warmer areas of the Earth absorbing more direct solar radiation. This means Earth-emitted IR radiation is heavily dependent on latitude with greater magnitude near the equator and lesser magnitude near the poles. Unlike how cloud cover increases albedo values, clouds and water vapor absorb IR radiation, decreasing the magnitude of Earth IR radiation emitted to space. Based on the same NASA/MSFC study, values of Earth IR radiation heat flux incident of a spacecraft varied from 108 W/m^2 < IR_{Earth} < 332 W/m^2 in Low Earth Orbit [9].

Spacecraft-Emitted Infrared Radiation

The exterior surfaces of the spacecraft not only absorb radiation from the space environment but also emit long-wavelength IR radiation in order to dissipate heat from

the spacecraft [8]. As discussed in the system thermal energy balance defined previously, emission of IR radiation from the spacecraft is the only method for the spacecraft to transfer heat out of the spacecraft. By the same methods, internal surfaces transfer heat to other internal surfaces within line of sight of each other, referred to as the view factor between surfaces, through IR radiation.

Surface Finish Effects on Radiation in Space

Due to the wavelength-dependence of the different types of radiation in space, thermal engineers utilize various wavelength-dependent coatings on surfaces of the spacecraft [8]. Surface finishes with low solar absorptivity and high emissivity, such as white paint, decrease the direct solar and albedo radiation absorbed by the spacecraft while increasing the absorption of Earth-emitted IR radiation and emission of IR radiation from the spacecraft. Finishes with low solar absorptivity and low emissivity, such as gold plating, decrease absorption and emission of radiation in all spectrums. Lastly, finishes with high solar absorptivity and high emissivity, such as black paint, increase the absorption and emission of radiation in all spectrums.

Conduction within the Spacecraft

The conduction network within the system is a critical piece of thermal control on the spacecraft. Conduction is used as a method to transfer heat from hot regions of the spacecraft towards the surfaces of the spacecraft emitting heat away from the spacecraft [8]. Without adequate conduction, the hot regions of the spacecraft could become too hot, which could cause component failures. A critical aspect of conduction performance within a spacecraft is the thermal contact resistance between two materials in contact [5]. Due to surface roughness or loose connections between materials such as

a loose bolt, there is a resistance across all connections between materials due to finite gaps between the surfaces. These gaps result in degraded conduction performance.

Spacecraft Thermal Analysis

As previously mentioned, most real-world thermal analysis problems are too complicated to utilize analytical techniques alone in order to accurately predict thermal performance. In general, the modes of heat transfer involved in an analysis problem dictate what types of numerical or computational methods are feasible. In this research, the Monte Carlo/Ray Trace Method for radiation determination and the Finite Difference Method for energy balance calculations will be utilized.

The Monte Carlo/Ray Trace Radiation Method

The Monte Carlo/Ray Trace method is utilized in order to determine the radiation heat flux emitted and absorbed by each node within the finite difference model. Ray tracing is the process of determining what surfaces would be in line of sight of radiation from a source and what angle the radiation heat flux would hit the surface [6]. For each of the sources of radiation, both from environmental and surface emission, a series of radiation exchange view factors is calculated for any orientation of each surface relative to the radiation source. It is important to note these calculations factor in potential diffusely emitted radiation from a surface, direct radiation from an environmental source, and radiation reflected by another surface.

Once all of the view factors for each of the surfaces are calculated, Monte Carlo simulations are run to determine the heat flux absorbed, reflected, transmitted, and emitted by each of the surfaces at a given time step. A Monte Carlo method is a

probabilistic method of running numerous simulations of a known process in order to determine the likely outcome of the process [6]. This can be applied to radiation heat transfer by treating the thermal radiation waves emitted by a source as a defined quantity of discrete packets of energy. The Monte Carlo simulations then utilize the previously calculated view factors and the specified optical properties to determine the likely amount of emitted radiation heat flux from any source that is absorbed, transmitted, or reflected by a surface. These heat flux values are then incorporated into the energy balance within the finite difference model in order to determine the surface temperatures at the given time step.

The Finite Difference Method

Unlike an analytical solution where the temperature at any point in a system is known at all times, a computational solution requires each part within the system to be divided into smaller discrete sections of the geometry considered nodes [5]. Depending on computational power, complexity of the system, and the level of detail at which temperatures must be known within the system, a user must determine the appropriate number of nodes for their application. The greater the number of nodes, the more computational power and time simulations will need and on the contrary, the finer detail the model will have.

Once the model is constructed and the nodal network of each of the parts is generated, a finite difference solution can be calculated. At each node, the temperature of the node and that of the adjacent nodes is compared to determine the conduction heat transfer between nodes [5]. The energy generation and storage in the node, as defined by user-input material properties, are factored in to determine the energy exchange between

the node and its surrounding nodes. The energy balances for each of the nodes is then solved simultaneously for each time step throughout the simulation as determined by the user.

Thermal Vacuum Chamber Environment

Purposes of TVAC Testing

A thermal vacuum chamber is a temperature-controlled chamber maintained at high vacuum pressure levels in order to test space hardware in a representative environment. The TVAC environment is the closest terrestrial simulation of the space environment. TVAC testing of space hardware is accomplished for one of two purposes: thermal vacuum qualification testing or thermal balance testing [11]. TVAC qualification testing entails a combination of tests at extreme hot and cold temperatures along with temperature cycling between these hot and cold temperatures. The overall goal of TVAC qualification testing is to determine the survivability and operability of each of the components and the spacecraft as a whole within the simulated space environment.

Thermal Balance Testing

Thermal balance testing is a combination of testing a spacecraft, subsystem, or component at the on-orbit worst-case cold and hot conditions, along with at least one other condition chosen by the thermal engineer for steady-state data correlation [11]. Data is also collected during the transition between these temperatures for use in transient data correlation. It is recommended to test with as close to on-orbit environmental conditions as practical. Thermal balance testing validates the thermal design and the thermal model of the test article. If the thermal model has accuracy issues, thermal

balance test data can be used to tune the model in order to improve model accuracy. Once the computational thermal model is validated, it can be used for predictions of untested scenarios including any planned on-orbit condition.

Proportional Integral Derivative Control

PID control is a type of closed-loop control with a system model shown in Figure 3. An error signal, the difference between the desired and actual parameter values, is sent back to the controller [12]. The controller then takes the derivative and integral of the error signal. As shown, the error, the integral of the error, and the derivative of the error are multiplied by control coefficients, or gain parameters.

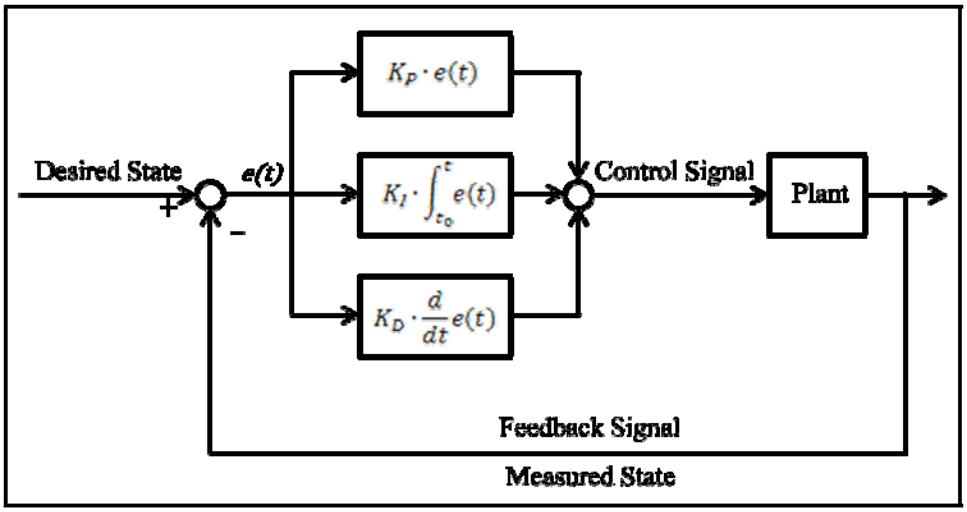

Figure 3 PID Control System Model

These three control signals are summed and sent as a control signal to the plant, or system being controlled. The values of each of the three control coefficients, proportional (K_P), integral (K_I), and derivative (K_D), are set by the operator and are extremely coupled in achieving intended performance parameters. Table 1 provides the general effects each of the control coefficients has on the controller performance.

While it is important to understand how each PID coefficient generally affects control performance, this only provides a general guideline for determining appropriate coefficients [12]. The coupled interactions between each coefficient and the control response of the plant make every application of PID control different.

Table 1 Effect of Increasing PID Control Coefficient on Controller Performance Parameters [12]

Coefficient	Rise Time	Overshoot	Settling Time	Steady-State Error
K_P	Decrease	Increase	Small Change	Decrease
K_I	Decrease	Increase	Increase	Eliminate
K_D	Small Change	Decrease	Decrease	No Change

A general process for manually tuning a PID controller is to start with proportional control in order to achieve the desired rise time, then add derivate control in order to reduce the overshoot and settling time as necessary. Lastly, add in integral control as necessary in order to reduce steady-state error. Throughout this process, iteration and trial and error are required in order to balance these coefficients to obtain desired response of all performance parameters.

Spacecraft Thermal Analysis and Test Research

Although nothing was found in published accessible research about developing a validated model of a TVAC for use in validating spacecraft TVAC models, the NASA General Environmental Verification Standards (GEVS) document implies the existence of this capability in its description of the use of thermal balance testing in order to validate a thermal model [11]. GEVS states "The models can also be modified to predict the thermal performance in a test-chamber environment. That is, the models are

frequently used, with appropriate changes to represent known test chamber configurations" [11]. As stated, organizations performing testing must have appropriately validated models of these known test chamber configurations in order for these model predictions to be accurate representations of TVAC testing conditions.

In 1994, Samson et al. at the Canadian Space Agency performed thermal balance testing on the MSAT spacecraft [13]. The test team accomplished five thermal balance phases to mimic different on-orbit conditions: transfer orbit, on-orbit storage, equinox at beginning of satellite life, and summer and winter solstice at end of satellite life. The team used IR lamps aimed at seven separately-controlled zones of the spacecraft to mimic on-orbit Earth IR radiation and direct solar radiation. They used a computer algorithm to control the heat flux on each of the seven zones of the spacecraft to mimic changes to the heat fluxes on each zone throughout the orbit. Although Samson et al. did not specify how they modeled the environment for generating their temperature predictions, they correlated test predictions to the environmental simulations performed on their thermal model.

In 2010, Jin et al. at the Nanyang Technological University in Singapore conducted thermal balance testing of a thermal test model of a 120 kg class micro-satellite [14]. They then correlated test data to the analytical thermal model of that thermal test model. The test team ran three analysis cases. The first two cases included eclipse scenarios in which an IR heater was turned on to simulate solar flux for the appropriate duration of the planned orbit and duty cycling of electronics related to the specific spacecraft modes tested. The first case tested the solar panel sun-pointing mode. The second case tested the nadir-pointing imaging mode. The third case was an extreme

hot case where two thirds of the equivalent solar flux was constantly applied with no simulated eclipse and all electronics turned on. Jin et al. minimally discussed that their analytical predictions were run with an analytical model of the test case environments, along with some uncertainty in the utilized environments. An example of effects not captured in their environmental predictions is that when they turned off the IR lamp, there was still some residual heat flux from the lamp until it cooled. There is also no discussion of validation of the experimental setup modeling in order to reduce and/or quantify this uncertainty. In order to upgrade their model to correlate with test data to within their predetermined $T_{error} \leq 5°C$ margin in all three cases, Jin et al. iteratively varied the thermophysical properties, optical properties, contact thermal resistance between surfaces, mounting of components, and equipment heat dissipation.

At the Massachusetts Institute of Technology, Richmond developed a thermal computational model in MATLAB® to bridge the gap between the inaccuracies involved in first-order estimates and the complexity of commercial software packages such as Thermal Desktop® [15]. Richmond was able to achieve model predictions within five percent error of predictions generated in Thermal Desktop®. Richmond generated on-orbit predictions to compare to the on-orbit predictions within Thermal Desktop®, but due to scope of his research, he was not able to generate predictions for a TVAC in order to compare predictions to test data. Richmond recommended this in the future work section of his research as a key component of model confidence.

In 2011 at the Naval Postgraduate School (NPS), Smith generated a thermal model of the NPS Solar Cell Array Tester (NPS-SCAT) nanosatellite [4]. Smith developed the thermal model in NX-6 IDEAS®, a finite element modeling thermal

software. Smith attempted to use TVAC test data to validate the thermal model. Hot soak predictions for the payload were accurate within $T_{error} \leq 2.5°C$, but significant unexplained discrepancies in temperature occurred during the cold soak test. The analytical model of the TVAC entailed the enclosure of the TVAC shroud. The shroud was modeled at a uniform temperature based on one thermocouple instrumented to the shroud during the actual test. No other interactions with the spacecraft, such as conduction with the platen, were modeled.

Specifically at AFIT in 2011, Urban used Thermal Desktop® in order to generate five predictive thermal models of small-satellite or CubeSat class spacecraft or thermal test models [16]. Urban then correlated TVAC test data to two of the thermal models he generated. Based on a method developed by another Thermal Desktop® user and posted on the software user forum, Urban generated a boundary node to model the radiation effects of the shroud of the TVAC. The temperature of this boundary node was varied with time to match the TVAC profile executed, similar to Smith's research. This boundary node has infinite capacitance, meaning the node can infinitely absorb all incident radiation at all wavelengths, and has no conduction to the spacecraft. Because no conduction was modeled, this model did not allow for the spacecraft to be placed on the platen within the TVAC. Urban was able to iteratively modify model properties in order to correlate the model to TVAC test data. Similar to test data correlation at Nanyang Technological University, the TVAC environment analytical model was not validated prior to use in model correlation.

Summary

This section provided an overview of the physical and mathematical concepts and published work pertaining to this research. In conclusion, the complexity of conduction and radiation analysis within a spacecraft requires computational modeling to provide accurate predictions. The computational methods used in this research provide the capability to factor in all thermal effects of the TVAC and on-orbit environments in generating a computational thermal model for design verification. Along with computational modeling, understanding the TVAC environment and how to manipulate it for spacecraft testing is a critical component of verifying the thermal design of a spacecraft or payload. Also, thermal testing is an effective way to validate computational thermal models, giving the thermal engineer the ability to use the model to predict untested conditions such as on-orbit scenarios. Available research provided a compelling case for developing a validated computational model of the TVAC environment for use in spacecraft computational model validation and in some cases, implied its existence in larger space programs and test facilities. All of these factors are included in the structure of the computational and experimental methodology of this research.

III. Methodology

Chapter Overview

This chapter provides the methodology of the experimental and computational approaches of this research. This research used experiments conducted within the AFIT Solar Simulation TVAC in order to characterize appropriate chamber usage techniques and highlight potential improvement areas of this unique design. Also, this same experimental data was used to validate a computational thermal model of the TVAC environment. First, this chapter describes the equipment, software, and test articles used to accomplish this research. Then a comprehensive description of experiments run as a part of this research is provided. Lastly, this chapter describes the modeling techniques and process utilized in order to develop, modify, and validate the TVAC computational thermal model.

AFIT Solar Simulation TVAC

The AFIT Solar Simulation TVAC is a 27x27x29.75 in (0.69x0.69x0.76 m) chamber designed and built by Abbess Instruments Inc., capable of pressures as low as $P = 8.51 \text{x} 10^{-9}$ Torr. It is comprised of a temperature-controlled gold-plated copper platen, four temperature-controlled copper walls coated with Aeroglaze®, and a copper door coated with Aeroglaze®, each of which is 0.5 inches (0.0127 m) thick. The shroud is coated with Aeroglaze® to model the highly effective absorption of long-wavelength IR of deep space. The platen and shroud create an interior shell within the sealed and insulated aluminum chamber as shown in Figure 4.

Resistance Temperature Detectors (RTD) and thermocouples are built into the chamber for temperature control of the platen as well as the shroud, which is composed of the walls and ceiling of the chamber. Five thermocouples are also fed into the chamber for use to measure temperatures on test articles as shown in Figure 5.

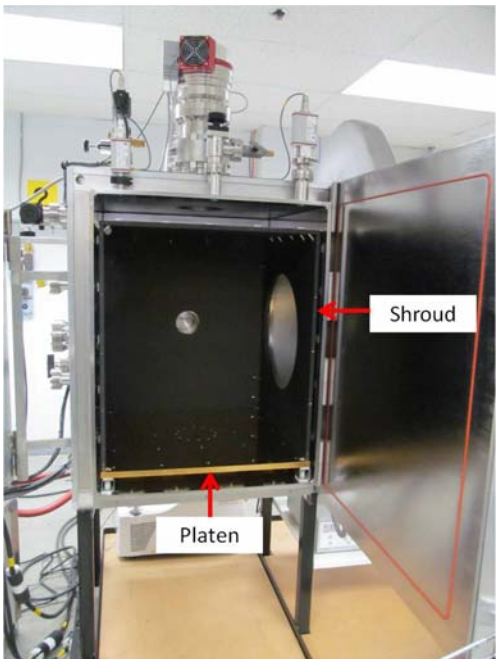

Figure 4 AFIT Solar Simulation TVAC Shroud and Platen

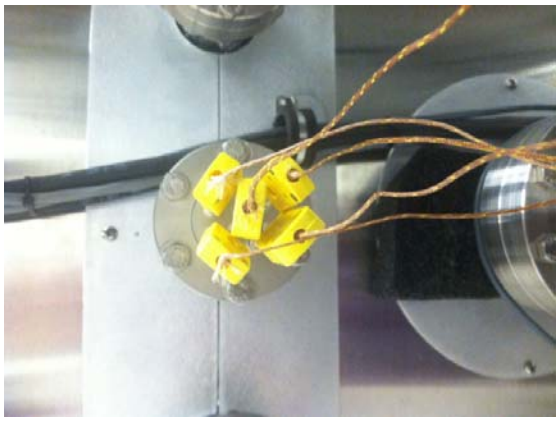

Figure 5 AFIT Solar Simulation TVAC Test Article Type K Thermocouple Pass Through

The platen and shroud are individually temperature controlled by respective ThermoFisher Scientific bath chillers pumping a working fluid through a fluid network on the exterior surfaces of the platen and shroud.

A solar simulator lamp shines a 12x12 inch (0.304x0.304 m) beam of one-sun equivalent collimated light into the chamber through a sealed quartz window. The solar simulator has shutter control capability for use in simulating orbit and eclipse durations during testing.

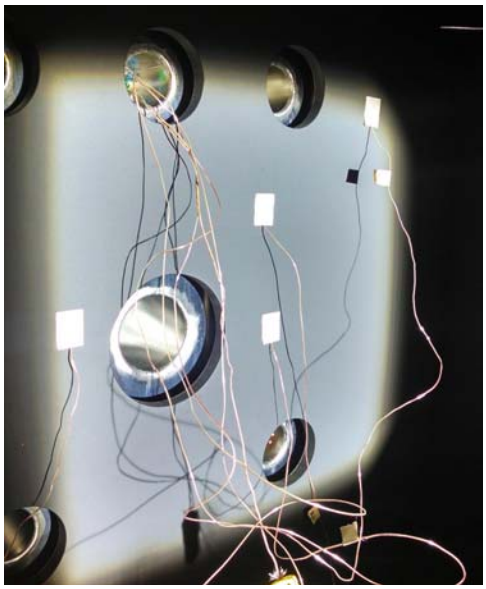

Figure 6 Left Shroud Wall Incident of Solar Simulator Instrumented with Thermocouples with Solar Simulator On

At the time of this research, the platen and shroud could reach a minimum temperature of T = -24°C and T = -20°C respectively. The TVAC has not been tested to maximum temperature capability as it is assumed to be a greater temperature than the limits of the black Aeroglaze® coating of the shroud walls, T = 135°C, and unnecessary

for meeting spacecraft qualification test objectives, due to the low likelihood of conditions at $T = 135°C$ to be experienced by a satellite on orbit.

Thermal Desktop®

Thermal Desktop® is a graphical user interface software suite built to work within AutoCAD® [17]. A user builds the geometric model within AutoCAD® and defines the nodal network of each of the parts within the system, including energy generation sources such as heaters. The user then defines the interfaces, called contactors, by which any parts in physical contact with each other conduct heat to each other. This creates the structure of the underlying mathematical model. The radiation environment the model will be exposed to is then generated within the software. The user can specify radiation hitting specific surfaces to mimic terrestrial environments such as a thermal vacuum chamber or one can specify orbital parameters for an on-orbit environment. If an on-orbit environment is selected, the user can program on-orbit slewing and maneuvering into the simulation in order to mimic the planned concept of operations (CONOPS) of the spacecraft. Once the radiation environment is setup, an analysis case is prepared, specifying the duration and time step of the simulation. The geometry of the model is then used to calculate the radiation exchange factors to be used in Monte Carlo simulations to determine environmental radiation heating rates on each node. Once the environmental heat rates are known for each time step, they are factored into the energy balance for each node, which is then used to simultaneously solve for nodal temperatures at each time step. The calculated radiation exchange factors are also used to determine emitted radiation exchange between nodes at each time step.

Test Articles

Aluminum Plates

One-quarter inch (0.0064 m) thick 6061-T6 aluminum plates of different surface area, 6 x 6 in (0.152x0.152 m) and 10 x 10 in (0.254x0.254 m), were utilized as test articles as shown in Figure 7. The surfaces of each plate were uncoated and untreated. The primary purpose of these test articles was to provide a basic correlation of thermal balance test data to model predictions. Since the plates have the same thermophysical and optical properties, they can be compared within the chamber with the only difference between the plates the known difference in dimension. If the TVAC computational model provides accurate predictions of the temperature of each plate, it would validate the TVAC computational model.

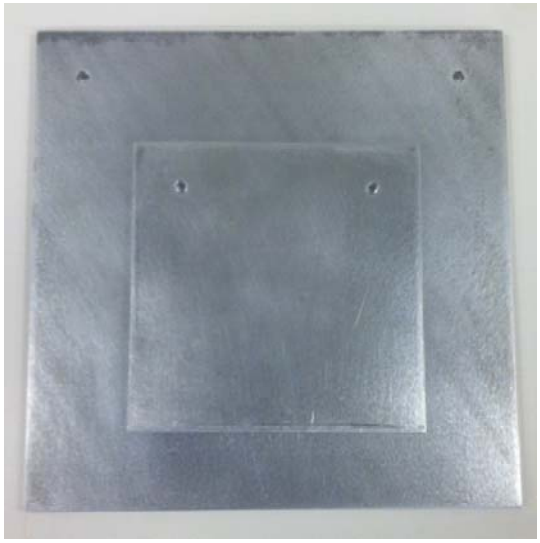

Figure 7 6x6 in and 10x10 in Aluminum Plates One Placed on Top of the Other

Experimental Methodology

For computational model correlation, it is ideal to be able to use only the built-in TVAC platen and shroud temperature sensors in order to apply the computational model of the chamber environment to the specific test cases executed in future spacecraft and payload thermal testing. This way, all five thermocouples would be available to measure data on the test article, not the chamber itself. With this goal in mind, steady-state and transient experimental methods were devised. Since experimental data for model correlation would also provide important information about how the TVAC performed, very few tests were needed beyond model correlation testing in order to characterize and improve chamber performance.

Tests were conducted to characterize each of the unique features within the TVAC throughout planned temperature profiles, specifically the platen, shroud walls, solar simulator gate valve flange and quartz window. The temperatures of each of the test articles were also measured throughout planned temperature profiles.

Temperature Control Methodology

Based on thermal balance testing discussed in Chapter 2, this research attempted to characterize both steady-state and transient effects within the TVAC environment. Since the three or more simulated scenarios or temperature set points for thermal balance testing of a given test article are completely dependent on the predicted on-orbit thermal environment for that test article, data was collected for four steady-state temperatures distributed throughout the chamber temperature envelope: T = -15°C, 10°C, 40°C, and 75°C. Transient data was collected during transitions increasing from the lowest to highest temperature, T = -15°C to T = 75°C, and decreasing from the highest to lowest

temperature, T = 75°C to T = -15°C. All temperature profiles were run at high vacuum pressure at $P < 10^{-6}$ Torr.

At each steady-state analysis temperature set point, the platen and shroud temperature controllers were held at those set points until the platen and shroud temperatures along with the instrumented temperatures reached a steady-state temperature and had a fluctuation of $|T_{fluc}| < 0.1$°C. This is how experimental steady-state temperature was defined for this research.

Characterizing and Improving Chamber Performance

Copper Plate Coated with Aeroglaze® to Mount to Platen

Since one of the purposes of the TVAC is to conduct orbital simulation with the solar simulator, it is important to setup an orbital simulation with as close to the space environment as possible. With a highly reflective gold platen, the TVAC provides an accurate mounting interface for the test of payloads which will be mounted on a reflective surface of a satellite bus. Since deep space is highly absorptive in long-wavelength IR and radiation emitted by a spacecraft is not reflected by deep space, the platen surface does not provide an accurate representation of deep space in terms of radiation for the test of a spacecraft. With this purpose in mind, this research was used to validate a design addition to the chamber. A copper plate was designed to mount to the platen and act as a black radiating surface for applicable orbital simulation testing. The copper plate would be coated with Aeroglaze® on the top side, to provide the same radiation properties as the shroud walls. The bottom side of the copper plate would be gold-plated in order to provide a smooth surface with low risk of oxidation for good thermal contact with the platen for temperature control.

For validation purposes prior to acquiring a surface-coated final product, a plain copper plate, shown mounted on the platen in Figure 8, was machined and tested to ensure the added plate would not inhibit conduction capabilities of the platen.

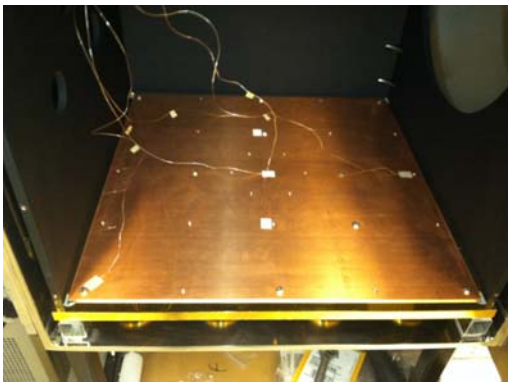

Figure 8 Copper Plate Bolted to Platen and Instrumented with Thermocouples

Since the fluid path of the platen temperature controller is well distributed along the bottom surface of the platen, the temperature of the bottom surface of the platen can be assumed to be approximately uniform at any point in time. Assuming the temperature of the bottom surface of the platen is approximately uniform and since the thicknesses of the platen and the copper plate are small relative to their depth and width, the transient conduction through the thickness of the platen and copper plate can be approximated by one-dimensional conduction. Since there is also no heat generation, Equation 4 can then be simplified as shown in Equation 16:

$$\frac{\partial^2 T}{\partial x^2} = \frac{1}{\alpha}\frac{\partial T}{\partial t} \tag{16}$$

Incropera et al. demonstrate how, for a semi-infinite solid, a similarity variable is used to convert Equation 16 from a partial differential equation with two independent

variables into an ordinary differential equation with one variable. The ordinary differential equation is then solved to determine a temperature difference through the depth of the material over time as shown in Equation 17 with boundary conditions given in Equations 18 and 19 [5]:

$$\frac{T(x) - T_{bottom}}{T_i - T_{bottom}} = erf\left(\frac{x}{2\sqrt{\alpha t}}\right) \quad \textbf{(17)}$$

$$T(x = 0, t > 0) = T_{bottom} \quad \textbf{(18)}$$

$$T(x, t = 0) = T_i \quad \textbf{(19)}$$

where x is the depth through the material from the bottom surface (m), T_{bottom} (K) is the constant temperature of the bottom surface of the material, T_i is the initial temperature at all locations within the material (K), and erf is the Gaussian error function.

This closed form solution provides a worst-case approximation of how long it would take for the top surface of the copper plate or the platen to reach the temperature of the bottom surface of the platen, once the bottom surface of the platen is held constant. Since this solution is for a semi-infinite solid, it assumes an infinite depth through the material; therefore, the semi-infinite solid solution assumes there is an infinite amount of copper on top of the platen or copper plate. As the temperatures of the platen and the copper plate change to converge towards the temperature of the bottom surface of the platen, this additional copper is at a temperature further from the temperature at the bottom of the platen.

For example, if the bottom surface of the platen is set to a constant temperature hotter than the platen and copper plate, the additional copper above the top surface of the platen or copper plate would be at a lower temperature than the platen and copper plate.

This means there would be energy consistently transferred from the platen and copper plate into this infinite depth of copper above them. This energy transfer causes the closed form prediction to predict a longer duration for the top surface of the platen or copper plate to reach the bottom surface of the platen temperature.

Since gold and copper have very low IR emissivity values, there is minimal energy transfer out of the top surface of the platen or copper plate in the actual case. This means that the vast majority of energy transfer into the platen and copper plate is from the temperature control fluid path on the bottom surface of the platen, which will decrease the duration for the top surface of the platen or copper plate to reach the bottom surface of the platen temperature as compared to this closed form predicted duration.

Additionally, Equation 17 demonstrates for any case a proportional relationship between the thickness of the material and the time required for the top surface to reach the bottom surface temperature as shown in Equation 20:

$$t \sim \frac{x^2}{\alpha} \tag{20}$$

Since an additional thickness x = 0.25 in (0.00635 m) is small along with the high thermal diffusivity of copper (α = 1.11x10^{-4} m^2/s [5]), the increase in time for the top surface of the copper plate to reach the bottom surface of the platen temperature relative to the same measurement for the top surface of the platen should be small as well. For example, if T_{bottom} = 0°C and T_i = -5°C, the closed form solution for the time it would take for the top surfaces of the platen and copper plate to be within ΔT = 0.5°C is $t =$ 3 minutes and $t =$ 6.7 minutes respectively. Since this is a worst-case approximation, the copper plate is unlikely to degrade conduction performance of

the chamber in an appreciable way, especially when compared to the hours and days time scale of TVAC testing

Addressing Risks of Solar Simulator Heating

As the AFIT Solar Simulation TVAC was a relatively untested new piece of equipment at the beginning of this research, the temperature increase on the left shroud wall, incident to the solar simulator beam of light, was unknown and a cause for concern as shown in Figure 6. The solar simulator was tested with no shroud cooling, with shroud cooling set at ambient temperature (T= 23°C), and the more likely configuration of the shroud being cooled at the minimum temperature the shroud is capable of being cooled to. Since the shroud is typically used to simulate the deep space environment and absorb IR radiation off of the test article, the lower the temperature of the shroud walls, the more realistically the TVAC environment emulates the orbital environment. The results of this test would be used for developing procedures for safe use of the solar simulator if restrictions were required.

PID Coefficient Tuning

Again, due to lack of previous testing of the chamber, the PID coefficients set by the manufacturer were not properly tuned for desired performance. Specifically, each temperature controller had substantial overshoot and would not settle to a steady-state value. Instead, the temperature controller would settle to a bounded oscillation larger than the previously prescribed $|T_{fluc}| < 0.1$°C bound.

PID coefficient tuning was done throughout the process of testing in order to get as close to desired performance, with small overshoot and a steady-state oscillation within $|T_{fluc}| < 0.1$°C. Since the Abbess Instruments-defined coefficients, shown in

Table 2, did not achieve desired performance, the ThermoFisher Scientific-defined factory default coefficients were tested first.

Table 2 Predefined PID Coefficients and Value Ranges

Coefficient	Abbess Value	ThermoFisher Value	Range of Possible Values
K_P	1	0.6	0.1-99.9
K_I	0.1	0.6	0.00-9.99
K_D	0	0	0.00-5.00

If there were any issues with the ThermoFisher Scientific coefficients, the process would be started with only proportional control, with derivative and then integral control added as required with iteration to achieve desired performance. It is important to note that platen controller performance may differ when a spacecraft or payload is inserted into the chamber since the additional thermal mass could dampen temperature oscillations in the controller. Due to the large mass of the copper shroud walls and platen relative to the small mass of CubeSats and small payloads, this effect is likely to be minimal.

Platen Testing

Without Copper Plate

Testing was accomplished on the platen to determine how the top surface temperature of the platen compared to the platen control temperature read on the bottom surface of the platen as shown in Figure 9. The platen was instrumented in an array to characterize any potential temperature gradients on the surface.

Figure 9 Platen Instrumented with Thermocouples

With Copper Plate

Testing with the copper plate mounted to the platen was to be repeated exactly the same way and with thermocouples positioned in the exact same locations as the test without the copper plate as shown in Figure 8. This was done in order to determine any changes to the platen's conduction capability with the addition of the copper plate.

Shroud Testing

Five Surfaces of Shroud

In order to characterize how the temperature of each of the five interior surfaces of the shroud compared to the shroud temperature read from the rear side of the back wall, the steady-state and transient temperature profile was run with each of the five walls instrumented as shown in Figure 10. Data from this experiment provides an understanding of any differences between the five surface temperatures along with an understanding of how these temperatures vary from the shroud control temperature.

The front wall of the shroud is of particular interest. Since the wall is removable in order to provide access to the chamber, this wall of the shroud is not thermally controlled other than through conduction where it is mounted on top of the platen and bolted to the top, left, and right shroud walls as shown in Figure 11.

Figure 10 Five Surfaces of Shroud Instrumented with Thermocouples

Figure 11 Front Wall of Shroud Bolted onto TVAC

One Shroud Wall Instrumented in Array

In order to ensure there are no significant gradients in temperature on the surface of a given wall of the shroud, the left side shroud wall was instrumented with all five thermocouples in an array to observe gradients on the surface as shown in Figure 6. During this test, extensive solar simulator testing was also conducted.

The solar simulator was tested with no shroud cooling, with shroud cooling set at ambient temperature (T = 23°C), and the more likely configuration of the shroud being cooled at the minimum temperature the shroud is capable of being cooled to. Since the platen is bolted to each of the shroud walls, the platen control temperature affects the shroud's cooling capability. In order to understand a realistic envelope for solar simulator operation, the platen was operated at T = -24°C and T = 50°C. This temperature envelope was modeled after the temperature range of the thermally-controlled plate AFIT's Space Object Self-Tracker payload will be mounted on, which could be assumed to be typical of a standard satellite bus [18], [19].

Solar Simulator Gate Valve Flange Testing

Between the shroud and the quartz window is a large pneumatic gate valve with a stainless steel flange. The flange was instrumented during platen testing as shown in Figure 12.

Since the solar simulation gate valve flange is not temperature controlled, it is important to understand how the rest of the chamber and the solar simulator impact its temperature. Without understanding the temperature profile of the flange, the TVAC environment computational model would be incomplete.

Figure 12 Solar Simulation Gate Valve Flange Instrumented with Thermocouple

Quartz Window Testing

The quartz window inset through the right side shroud wall, where the solar simulator light source is located, was instrumented during the one shroud wall array test as shown in Figure 13.

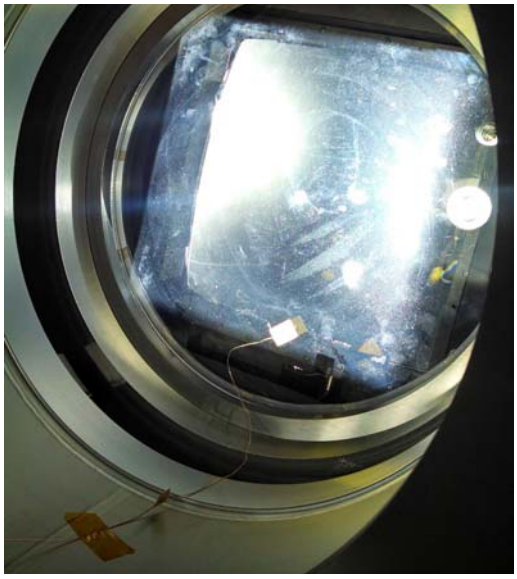

Figure 13 Quartz Window Instrumented with Thermocouple

Similar to the gate valve flange, the quartz window is not temperature controlled. Because of this, it is important to understand how the rest of the chamber impacts window temperature. While quartz transmits visible light very well, it has high IR emissivity. Since the surface of the quartz window is likely to be incident of a test article, especially if the solar simulator is used, it is important to accurately characterize the temperature of the surface of the quartz window, especially given its high IR emissivity. It is important to note that the quartz window temperature used for computational model development was measured without solar simulation. Had the solar simulator been turned on, the thermocouple would not have been measuring the window temperature but instead would have been measuring the temperature of the thermocouple itself as it absorbed incident solar flux through the quartz window. In order to potentially characterize the temperature of the quartz window as a part of adding solar simulation to the computational model, the solar simulator could be turned off briefly and the temperature of the thermocouple measured once the temperature of the thermocouple changes to a more steady value.

Aluminum Plates Testing

Each aluminum plate was suspended in the chamber by nylon monofilament fishing line tied to an 80/20® aluminum test stand set on the platen in the chamber as shown in Figure 14. The nylon was used in order to effectively thermally isolate the plate from the test stand and the platen, meaning there was negligible conduction between them. These tests provide data on basic test articles with common material properties for use in validating the TVAC computational model.

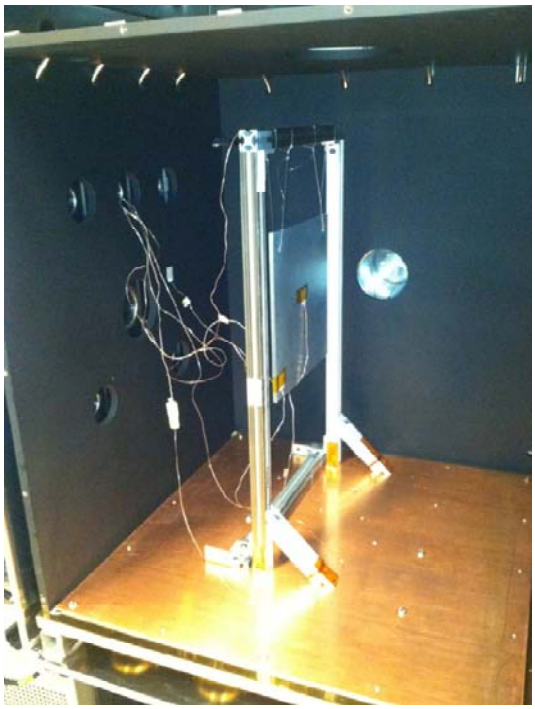

Figure 14 10x10 in Aluminum Plate Suspended from Test Stand in TVAC

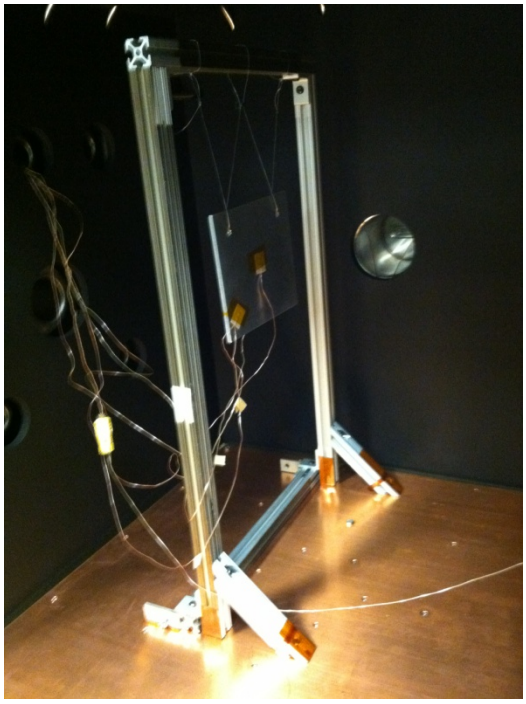

Figure 15 6x6 in Aluminum Plate Suspended from Test Stand in TVAC

Computational Modeling Methodology

This section overviews the modeling techniques of note specifically used to develop the computational models of the TVAC environment and test articles for this research in Thermal Desktop®. Urban provides a detailed summary of computational modeling in Thermal Desktop®, and the Thermal Desktop® User's Manual and Advanced Modeling Guide provide all information relevant to software use [16], [17], [20]. All values for thermophysical and optical properties of materials and surfaces were initially input based on best known values for each parameter of a given material. Changing these parameters is one of the techniques used to attempt to correlate the experimental data to the computational thermal model, as many of these properties have variability from published values.

Computational Modeling of the TVAC Environment

Platen Model

The platen was modeled as a finite difference solid. A finite difference solid provides a capability a finite difference surface lacks. While a finite difference surface factors in the thickness and mass of the material it is modeling, conduction within the surface is only two-dimensional and does not account for conduction in the direction of the thickness of the material. A finite difference solid factors in three-dimensional conduction, which is applicable to the platen. Since the known temperature of the platen is on the bottom, the easiest way for a future user to apply a temperature profile to the platen for TVAC environment computational predictions is to use this known temperature parameter over time as the user input. This data is readily available from the TVAC when testing is complete and can be imported into Thermal Desktop®.

Shroud Model

The shroud walls were also modeled as finite difference solids. Although there is no conduction from the shroud walls to drive the need for three-dimensional conduction, the only known temperature for a given test profile is located on the back surface of the rear shroud wall. The easiest way for a test article computational model to be input into the TVAC environment computational model for a given test profile is to use that input temperature from the back side of the rear shroud wall to control the temperatures of the rear surface of each of the walls. The temperature input is setup as a boundary node conducting to the rear surface of each of the four temperature-controlled shroud walls. Any temperature differences between the walls discovered during testing can be factored into controlling the different walls with a different contact resistance from the input temperature boundary node. All of the shroud walls are connected with contactors to model the contact resistance across the wall joints. The contact resistances along each wall joint was a primary design variable for developing an accurate computational model of the TVAC environment compared to experimental data.

The shroud wall with a circular hole in it was modeled as a wall with a square hole in it due to geometric modeling constraints for finite difference solids in Thermal Desktop® as shown in Figure 16. The square was cut out to have the same surface area and volume as the actual cutout. This change of shape could potentially have an effect on optical model accuracy, which was an accepted risk of this model.

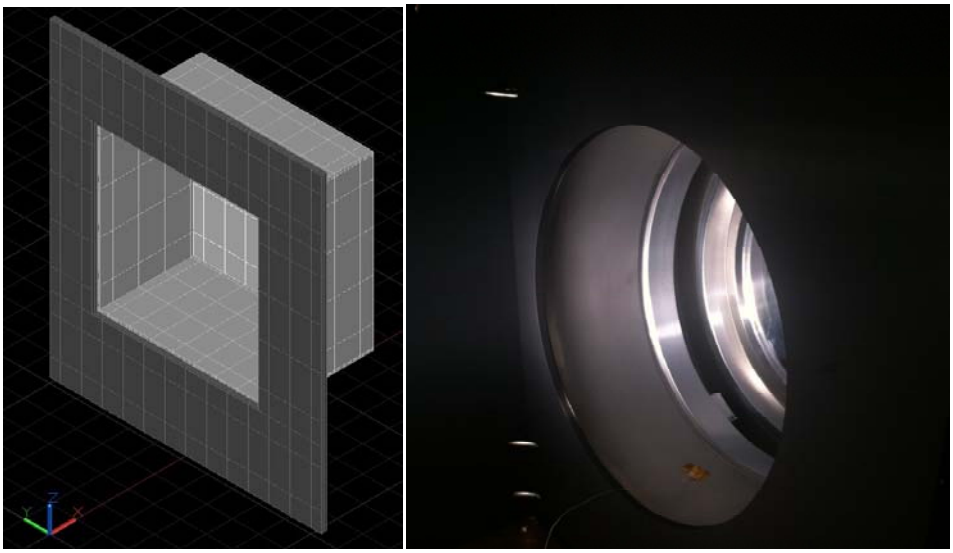

Figure 16 Right Shroud Wall and Solar Simulator Flange Computational Model Compared to Actual

The front shroud wall is only controlled in the model through conduction from the left, right, and top shroud walls, along with the platen. The front shroud wall also has energy losses from radiation emitted from its rear surface, which is absorbed by the TVAC door and lost from the system. A radiation boundary node was modeled in order to compensate for these losses. A radiation boundary node acts as a radiation absorber and emitter at a preset value input by the user. Steady-state data can be used to determine the parameters for this node based on known steady-state temperature differences on the front shroud wall relative to the other walls of the shroud. Although there are also radiation losses on the rear surface of each of the other shroud walls, it is assumed that these losses are compensated for by the shroud temperature controller on the same rear surface along with the fact the temperature is known at this location and input into the model from this location.

Solar Simulation Gate Valve Flange Model

The stainless steel solar simulation gate valve flange was modeled as a combination of finite difference solids as shown in Figure 16. The adjacent nodes of each finite difference solid were merged so the computational model would treat the combination of solids as one solid body. Since the exterior of the flange is exposed to ambient air, a natural convection boundary node was setup in order to model these effects.

Quartz Window Model

The quartz window was also modeled as a finite difference solid of the exact dimensions to fit within the end of the flange. Similar to the flange, the exterior of the quartz is exposed to ambient air, so natural convection was modeled in the same way as the solar simulation flange.

Integrated Model

Once each subset of the TVAC environmental model is built, they must be integrated to provide the appropriate coupled effects for potential predictions. The shroud walls are connected to the platen by contactors, modeling the contact resistance across the joints. The solar simulation flange and the quartz window are connected to each other with a contactor as well in order to model the contact resistance across the joint. Since there is no contact between the shroud and the gate valve flange, no conduction between the two was modeled. The entire TVAC environment computational model integrated together is shown in Figure 17.

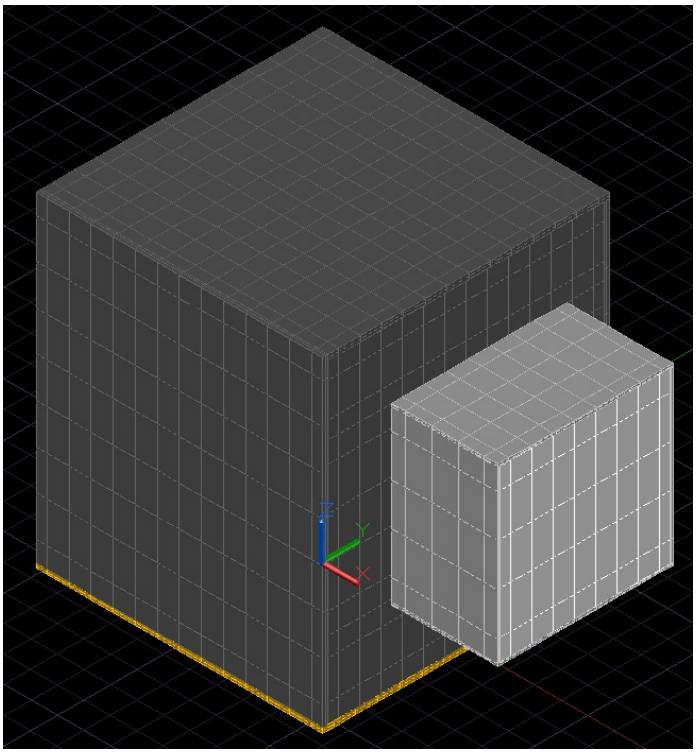

Figure 17 TVAC Environment Computational Model

Computational Modeling of Test Articles

Aluminum Plate Models

Each plate was modeled as a finite difference solid, in order to provide three-dimensional conduction. The test stand used to suspend the aluminum plates above the platen is incorporated into the model also as a finite difference solid. With two different geometry test articles with the exact same optical and thermophysical properties, computational simulations can be validated if the predictions for both plates are accurate using the same properties for each. Since each of the plates is one-quarter inch thick, the thickness of each of the plates was modeled with a grid size of two nodes, which should provide adequate modeling of conduction through the thickness, given the thermal conductivity through aluminum and assumed slow temperature changes to the aluminum

plate due to radiation from the TVAC environment. The 10x10 in aluminum plate and test stand model are shown in Figure 18

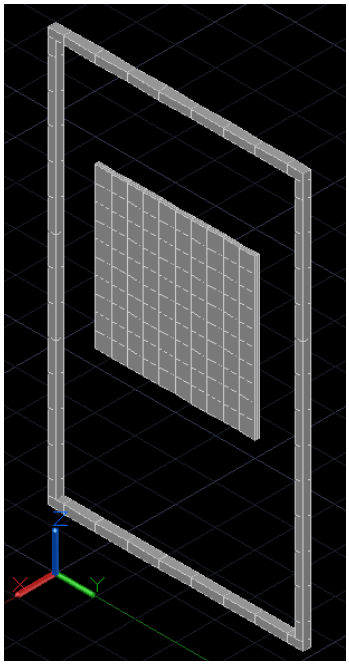

Figure 18 10x10 in Aluminum Plate and Test Stand Computational Model

Computational Model Correlation to TVAC Experimental Data

Steady-State Model Correlation

For every steady-state temperature set point, each of the temperature measurements provides critical information about the test article's interactions with the chamber. Based on established conduction and radiation principles, steady-state analysis provides critical data to be used to validate computational model parameters for conduction interfaces, material thermophysical properties, and surface optical properties. For any issues within the steady-state computational thermal model, these properties can be modified in order to rectify any errors. Strong correlations, within $T_{error} \leq 3°C$, between the computational prediction and experimental data provide substantial

confidence in the computational models of both the environment and the test article [8]. Correlations with an error of $T_{error} \leq 5°C$ are still considered acceptable for model correlation.

Transient Model Correlation

Once the computational model is correlated to steady-state data, it is important to also verify the computational model is also effective for transient scenarios. This is because all on-orbit scenarios for predictions are transient since the spacecraft's orbital thermal environment is constantly changing throughout the orbit. For transient temperature data, Thermal Desktop® provides the capability to run simulations given environmental temperature inputs. The temperature of each node is then plotted for every time step within the simulation. The same computational model properties as were used for steady-state correlation can be modified in order to match data to predictions. Once there is at least acceptable correlation, it is important to ensure this has not worsened steady-state data correlation.

Summary

This chapter provided an overview of the experimental and computational methodology of this research. Also, this chapter provided an overview of the test equipment and test articles for this research, along with planned characterization and improvement of the TVAC. The computational modeling techniques applied along with the experiments chosen for this research developed the capability to generate predictions and results for analysis and correlation.

IV. Analysis and Results

Chapter Overview

This chapter presents analysis and results of the experimental and computational methodology executed as outlined in Chapter III. First, this chapter provides an overview of uncertainty and outlines any anomalies with data collection. Then an overview of TVAC performance characterization is provided, and improvement methods are discussed within the outlined areas of interest. Lastly, the TVAC computational model is compared to experimental data to determine viability of the model for the tested scenarios.

Uncertainty of Experimental Data and Data Collection Anomalies

Throughout the experimental process of this research, there were multiple occasions in which data acquisition failed during testing, resulting in lost data for portions of completed tests. This was due to power issues with the laptop connected to the data acquisition setup for the test instrumentation thermocouples and also due to data logging script errors when a new computer was setup to replace the malfunctioning one. Other instrumentation was inaccurate for periods of specific tests because the adhesive holding a given thermocouple in place did not hold for the duration of the test. These errors were noted, and this research works to use all of the properly collected data to fulfill the objectives. Due to duration of TVAC tests on the order three to five days in length, tests with data collection anomalies were not necessarily able to be rerun within the time frame of this research.

Characterizing and Improving Chamber Performance

Copper Plate Coated with Aeroglaze® to Mount to Platen

Due to data acquisition power losses and thermocouple adhesive failures, platen data using the general planned temperature profile had significant error or data losses. Previous data was available from an initial test which was run in the early phases of this research in order to analyze the effect on conduction of adding the copper plate to the platen. The temperature profile for these supplemental experiments included three cycles of changing the temperature of the platen between T = -5°C and 75°C. Although each of these experiments did not achieve steady-state temperatures at any of the time steps, strong transient correlation between the bottom of the platen and the instrumented temperatures can provide confidence in assuming what the steady-state temperatures of the instrumented locations would be. Figures 19 and 20 show the measured temperature of the top of the platen and the top of the copper plate respectively as compared to the temperature of the bottom surface of the platen for their respective tests. Due to the difference in ramp rates of the platen temperature controller due to the thermal mass of the copper plate, the platen and copper plate data are not directly comparable to each other. Instead, the difference between these temperatures relative to the bottom surface of the platen temperature were compared.

The top of the platen had a temperature difference from the bottom of the platen of $\Delta T < 4$°C. Similarly, the top of the copper plate had a temperature difference from the bottom of the platen of $\Delta T < 3$°C. As expected, the temperature of the top of the copper plate had a larger time lag than the top of the platen temperature relative to the bottom of the platen temperature, while neither time lag was significant.

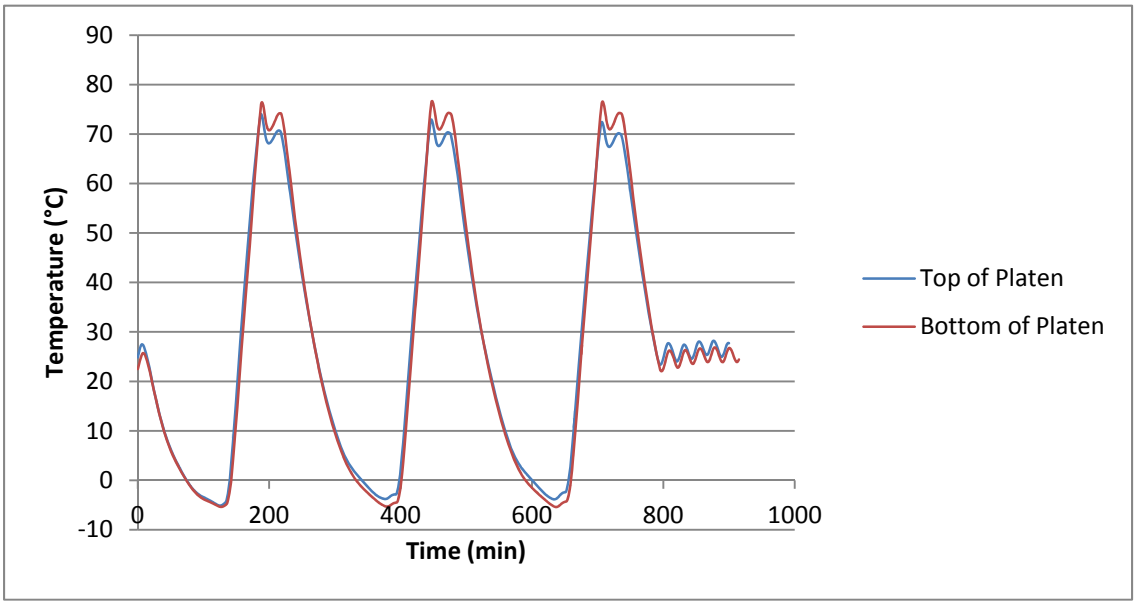

Figure 19 Temperature of Top and Bottom of Platen with No Copper Plate

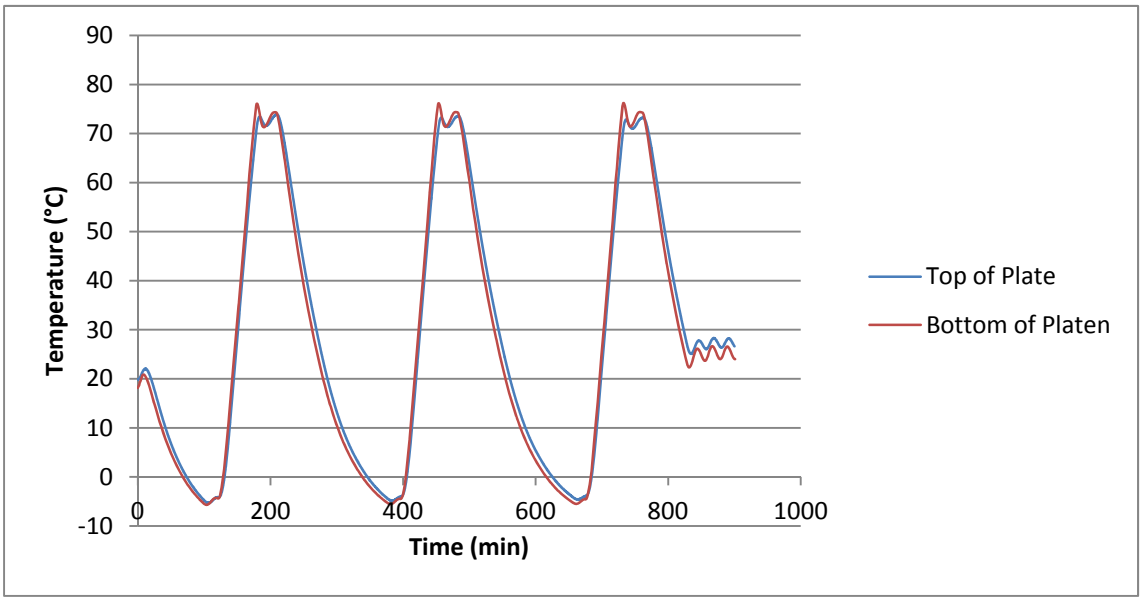

Figure 20 Temperature of Top of Copper Plate and Bottom of Platen with Copper Plate Attached

Also, the added thermal mass of the copper plate mounted to the platen caused the platen controller to take $t = 71$ minutes to increase the bottom of the platen temperature

from T = -5°C to T = 75°C as opposed to t = 60 minutes without the copper plate attached. Treating the bottom surface of the platen temperature as a boundary condition for conduction from the bottom of the platen through to the top of the platen and then the top of the copper plate, a slower ramp rate of the bottom surface temperature has an effect on how quickly the top of the copper plate reaches the same temperature as the bottom of the platen. Since the bottom of the platen surface temperature increases more slowly with the copper plate attached, transient conduction through the platen and plate had more time to change the temperature of the top of the copper plate relative to the bottom of the platen temperature. This potentially enhanced the top of the copper plate's comparative ability to track the temperature of the bottom surface of the platen.

Figure 19 demonstrates how the top surface of the platen temperature tracks with the controller oscillations in the bottom of the platen temperature, while Figure 20 demonstrates how the top of the copper plate temperature tracks these control oscillations more slowly. At the minimum and maximum temperatures, the top of the copper plate appears to track the bottom surface of the platen temperature better than the top of the platen. This demonstrates that the top of the copper plate is less sensitive than the top surface of the platen to temperature changes at the bottom surface of the platen from the controller due to the mass difference discussed previously.

While the addition of the copper plate slowed the ramp rate of the platen bottom surface temperature, the copper plate did not degrade conduction from the platen bottom surface through to the top surface of the copper plate. As long as a longer temperature ramp rate is acceptable, the top of the copper plate temperature provides negligible loss in capability to match platen bottom surface temperatures over hours and days time scales

of TVAC tests. This means the addition of a copper plate coated with Aeroglaze® to provide different optical properties for the platen surface within the TVAC is feasible. This plate could provide more accurate simulation of deep space optical properties for tests with the test article suspended off of the platen. Also, if payloads are planned to be mounted on a black surface of a satellite bus, the copper plate could be used to simulate these optical properties of the mounting surface. Lastly, similar copper plates could also potentially be fabricated and coated to accurately simulate other payload mounting surface types.

Addressing Risks of Solar Simulator Heating

During the test with one shroud wall instrumented in an array, the solar simulator was tested to determine the risk of damaging the Aeroglaze® coating on the shroud wall incident the solar simulator flux. The solar simulator was first tested with the shroud temperature controller set to hold the rear shroud wall surface temperature at $T = 23°C$ in order to ensure the solar simulator flux did not increase in temperature in an unsafe way with cooling on. After confirming incident wall temperatures were safe with temperature control, the temperature controllers were turned off in order to determine how quickly the solar simulator would heat the wall. The temperature limit for the shroud walls is $T = 135°C$, based on the temperature limit of the Aeroglaze® coating. Figure 21 shows the hottest temperature value measured on the front wall of the shroud as well as the back wall temperature while the solar simulator was on with no temperature control.

In order to quantify the worst-case scenario of how long it would take for the wall to heat up to $T = 135°C$, the slope of the line at the end of the data collection can be used to extrapolate the temperature change over time. The rate of temperature change would

be expected to increase at a slower rate than this as the rate of shroud wall temperature increase should decay over time due to inherent losses in the system, especially at higher temperatures. Figure 22 shows the worst-case ramp rate of the incident shroud wall temperature.

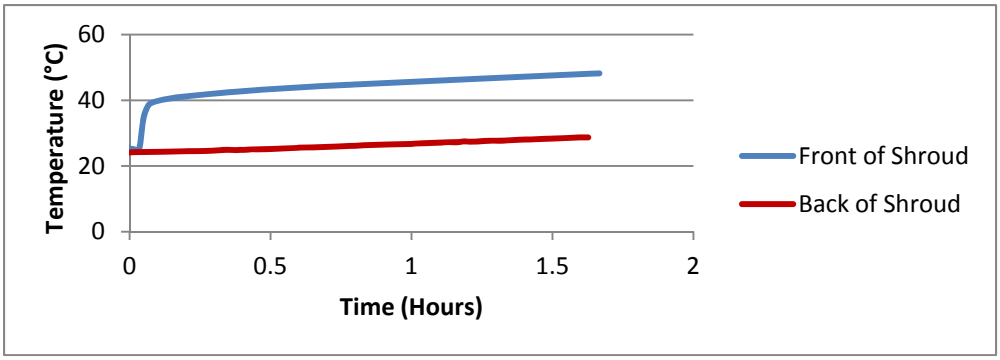

Figure 21 Temperature of the Front and Back of Incident Shroud Wall with Solar Simulator On and No Cooling

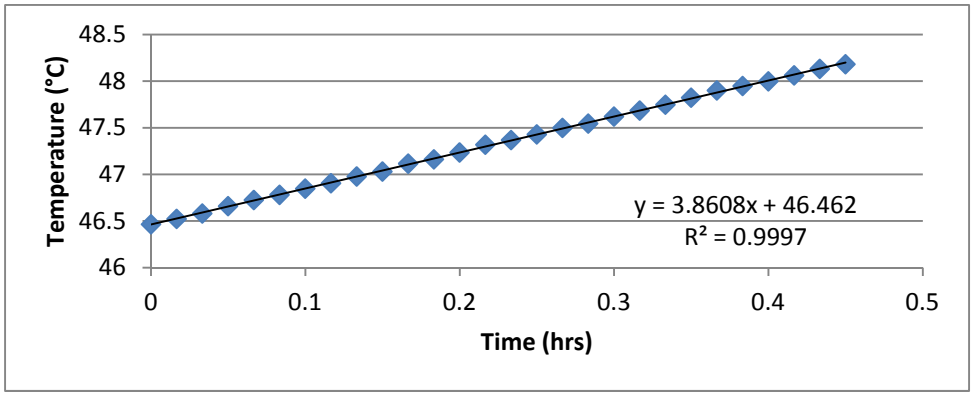

Figure 22 Worst-Case Temperature Ramp-Rate of Incident Shroud Wall with Solar Simulator On and No Cooling

With a maximum ramp rate of $\frac{dT}{dt}$ = 3.86°C/s, the incident wall temperature would take a minimum of t = 24.5 hrs in order to reach the temperature limit starting at room

temperature. With the assumption that the experiment is monitored at least once per morning or evening and that this is an absolute worst-case prediction, the fact the temperature controllers were not turned on would be discovered well before the temperature threshold was crossed. Given this assumption, no other local procedures need to be written in order to avoid damaging the Aeroglaze® coating.

PID Coefficient Tuning

PID coefficients of the temperature controllers were analyzed and then modified iteratively throughout early testing in the TVAC. Initial testing using the Abbess Instruments-defined coefficients shown previously in Table 2 demonstrated the need for controller tuning. An example of the oscillation of the controller attempting to track a steady-state set point at $T = 20°C$ is shown in Figure 23.

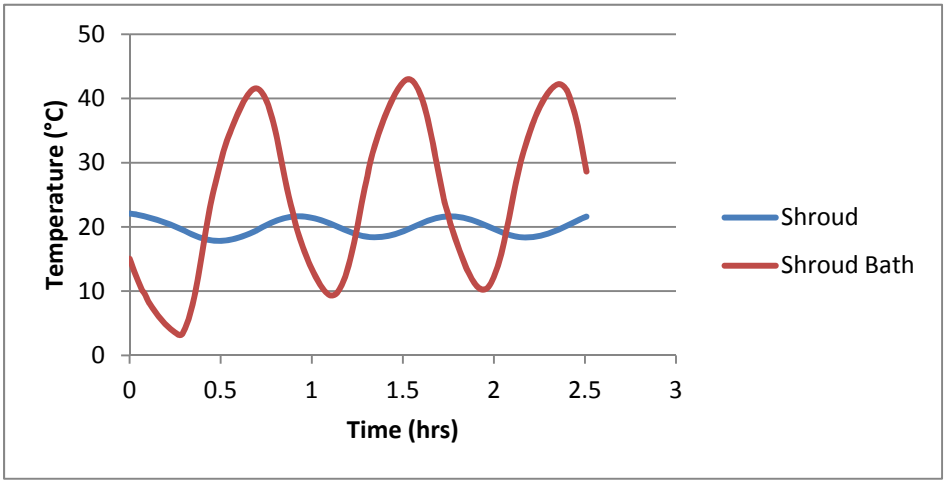

Figure 23 Shroud Controller Performance with Abbess Instruments-Defined Coefficients

The shroud controller is changing the bath temperature rapidly in order to maintain the shroud temperature within a bounded oscillation of $|T_{fluc}| < 2.2°C$, a larger oscillation than the desired bound for steady-state analysis.

Similarly, the ThermoFisher Scientific-defined coefficients from Table 2 had a bounded oscillation of $|T_{fluc}| < 1.7°C$ as shown in Figure 24. Since neither set of default PID coefficients provided the necessary settling time and steady-state error for steady-state measurements during thermal balance testing, the PID coefficients were tuned with the previously described method.

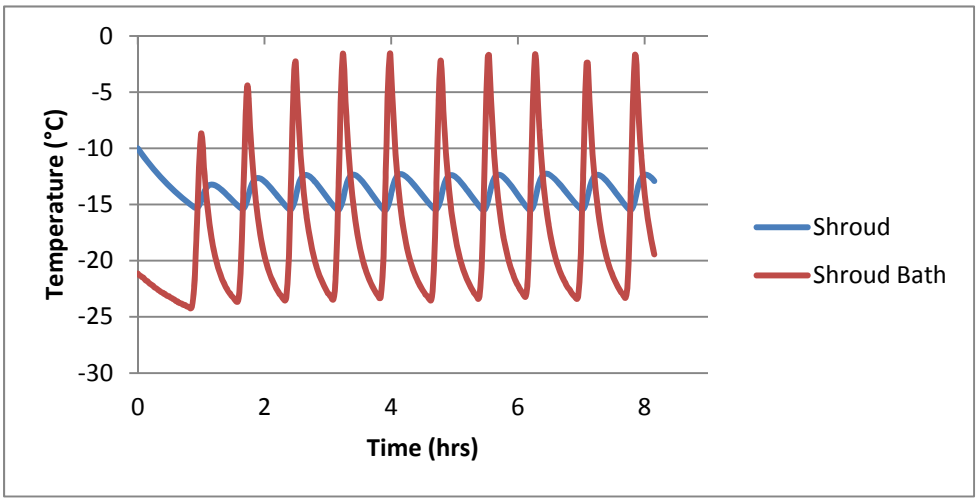

Figure 24 Platen Controller Performance with ThermoFisher Scientific-Defined Coefficients

Compared to the Abbess Instruments-defined proportional gain $K_P = 1$, the ThermoFisher Scientific-defined proportional coefficient value $K_P = 0.6$ demonstrated a negligible difference with rise time with a small decrease in overshoot and steady-state error. For this reason, $K_P = 0.6$ was chosen. Proportional-only control provided a large decrease in the bounded oscillation amplitude. With $K_P = 0.6$, the shroud controller kept

the temperature fluctuation within $|T_{fluc}| < 0.15°C$ as shown in Figure 25. Although the fluctuation is closer to the steady-state goal once integral control is removed, derivative control was necessary in order to dampen the temperature oscillation in the controller.

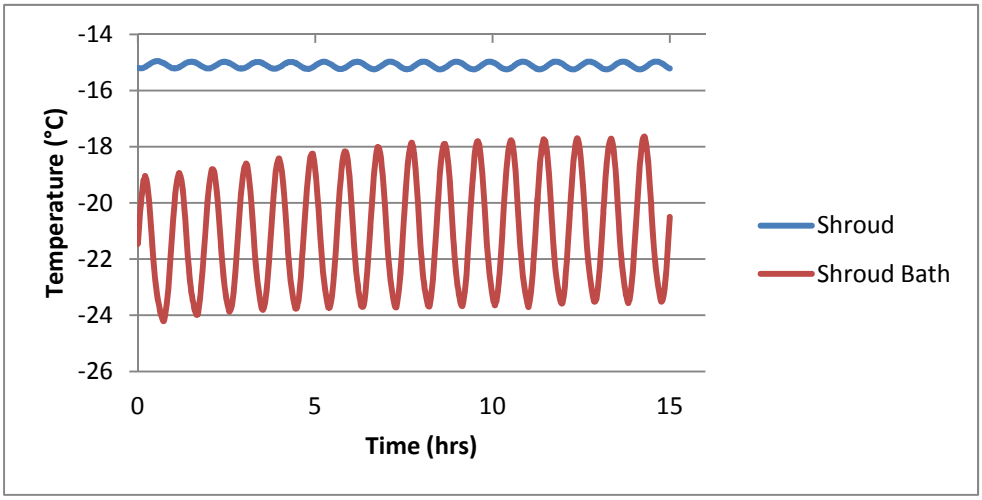

Figure 25 Shroud Controller with K_P = 1 Proportional Control

For proportional-derivative control, K_D = 5 was chosen since the maximum derivative gain did not have any negative effects on controller effects and had the maximum effect at dampening bounded oscillation as shown in Figure 26. Proportional-derivative control decreased temperature fluctuation to $|T_{fluc}| < 0.03°C$. The only deficiency with this control method was a controller steady-state error of $e_{ss} = 0.73°C$, which could be compensated for by changing the temperature set point if necessary.

The controllers were not truly optimized and performance likely could be improved with extensive analysis. This control scheme accomplishes the objectives of TVAC temperature control satisfactorily. Due to the size of the bath relative to the thermal mass and the fluid path length of the platen and shroud along with the bath controller heating and cooling capability, temperature set point overshoot and slow

temperature rise times were unavoidable. An improved controller with a larger bath size would be able to provide faster temperature rise time and settling time with less overshoot.

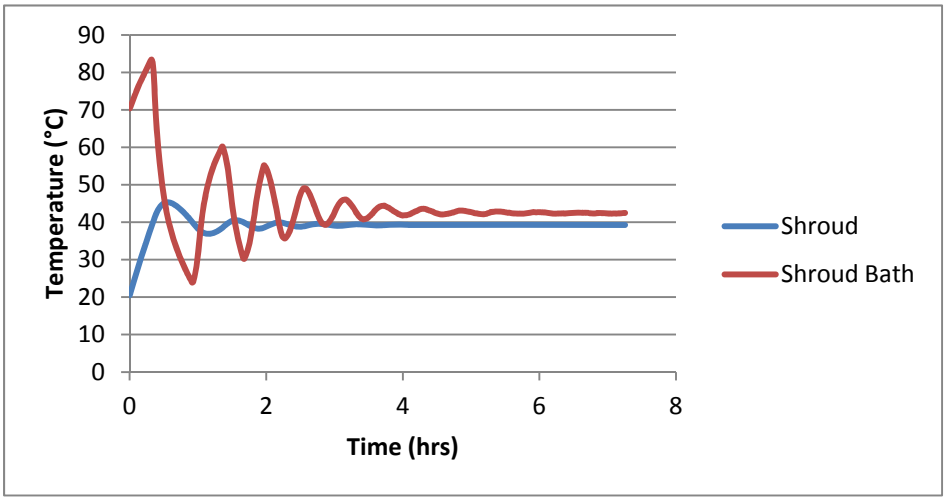

Figure 26 Shroud Controller with K_P = 0.6, K_D = 5 Proportional-Derivative Control

Computational Modeling of the TVAC Environment

TVAC Environment Model

Based on experimental data, the temperature-controlled platen and shroud walls are appropriately modeled as finite difference solids with a two-node depth across the thickness of each wall. Since temperatures of the top of the platen and the inside surfaces of the shroud closely followed the respective platen and shroud control temperatures as shown in Figure 19 and had experimental steady-state temperatures that matched the control temperature, this was deemed sufficient.

The key components to focus on within the TVAC environment computational model were the front shroud wall, the quartz window, and the solar simulation flange

since their temperature is not directly controlled by the fluid path. The steady-state temperatures for each of these components at each set point in the planned profile are displayed in Table 3. Solar simulator flange data was lost for two of the temperature set points, and steady-state temperature is listed as unknown at those temperatures

Table 3 TVAC Environment Steady-State Temperatures (°C)

Platen and Shroud Set Point T = -15°C			
Component	Predicted	Actual	T_{error}
Front Shroud Wall	-9.4	-10.4	1
Quartz Window	13.5	13.2	0.3
Solar Simulator Flange	20.4	16.5	3.9
Platen and Shroud Set Point T = 10°C			
Component	Predicted	Actual	T_{error}
Front Shroud Wall	13.2	12.1	1.1
Quartz Window	20.1	20.8	0.7
Solar Simulator Flange	23.1	Unknown	Unknown
Platen and Shroud Set Point T = 40°C			
Component	Predicted	Actual	T_{error}
Front Shroud Wall	40.2	39.8	0.4
Quartz Window	32.2	31.4	0.8
Solar Simulator Flange	29.8	Unknown	Unknown
Platen and Shroud Set Point T = 75°C			
Component	Predicted	Actual	T_{error}
Front Shroud Wall	71.6	71.9	0.3
Quartz Window	47.2	45.8	1.4
Solar Simulator Flange	38.2	41.2	3

For the entire TVAC model, steady-state temperature predictions from the TVAC environment computational model deviated from measured data by $T_{error} < 4$°C. While these values have acceptable accuracy, only the solar simulator flange predictions had an error of $T_{error} > 1.4$°C. This means the front wall of the shroud and the quartz window

steady-state predictions from the TVAC environment computational model provide a strong correlation, $T_{error} \leq 3°C$, to the measured data during testing. This is important to note because the solar simulator flange is likely to have less of an effect on a test article within the TVAC than the front wall of the shroud or the quartz window. This is because the normal of the surface of the entire solar simulator flange is incident of the solar simulator flange itself. Any effects the flange would have on the test article would be from reflection, which would not be dependent on temperature of the flange, and on the fractions of diffusely emitted radiation from the solar simulator flange absorbed by the test article.

Figures 27 and 28 show the transient computational predictions for the front wall of the shroud as compared to the measured data with increasing and decreasing temperature respectively. The transient results for the front wall of the shroud had a strong correlation with an error of $T_{error} < 2.4°C$.

Figures 29 and 30 show the transient computational predictions for the quartz window as compared to the measured data with increasing and decreasing temperature respectively. The transient results for the quartz window had an error of $T_{error} < 5.4°C$. While these values do not meet the objective for acceptable correlation of $T_{error} \leq 5°C$, the model has an error of $T_{error} < 4.7°C$ for the decreasing temperature prediction. Also, the increasing temperature transient prediction is only outside of $T_{error} \leq 5°C$ for 4.5% of the temperature transition before the model begins to match the measured data with an acceptable correlation again.

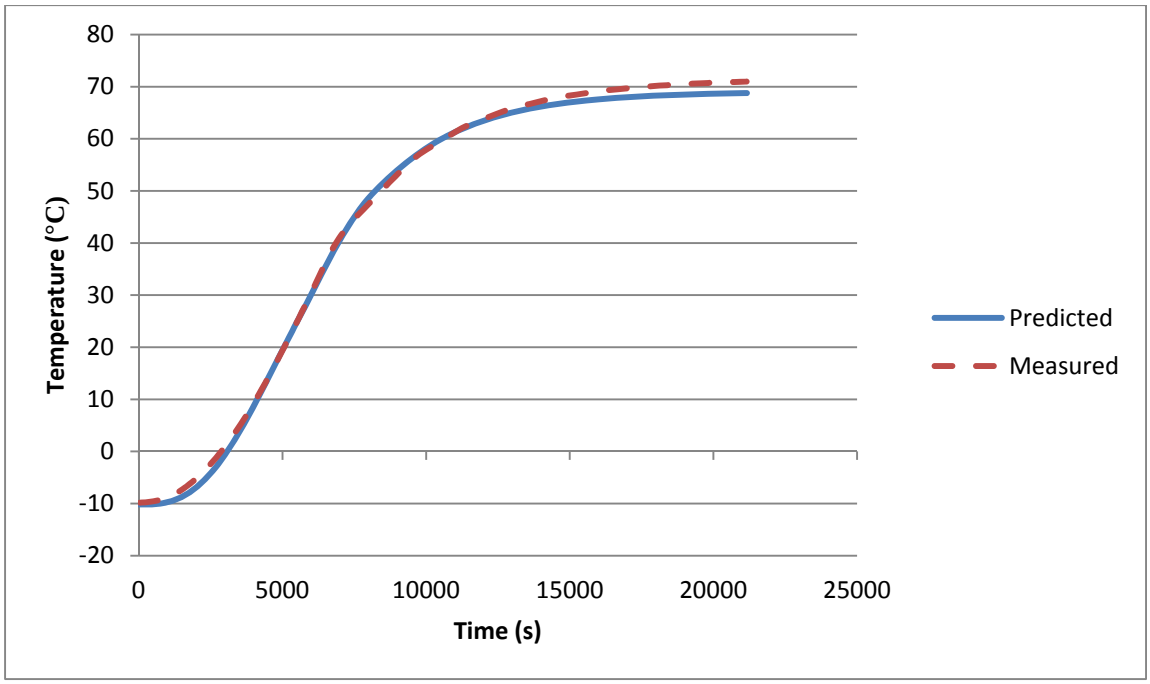

Figure 27 Front Wall of Shroud Increasing Temperature Transient Results

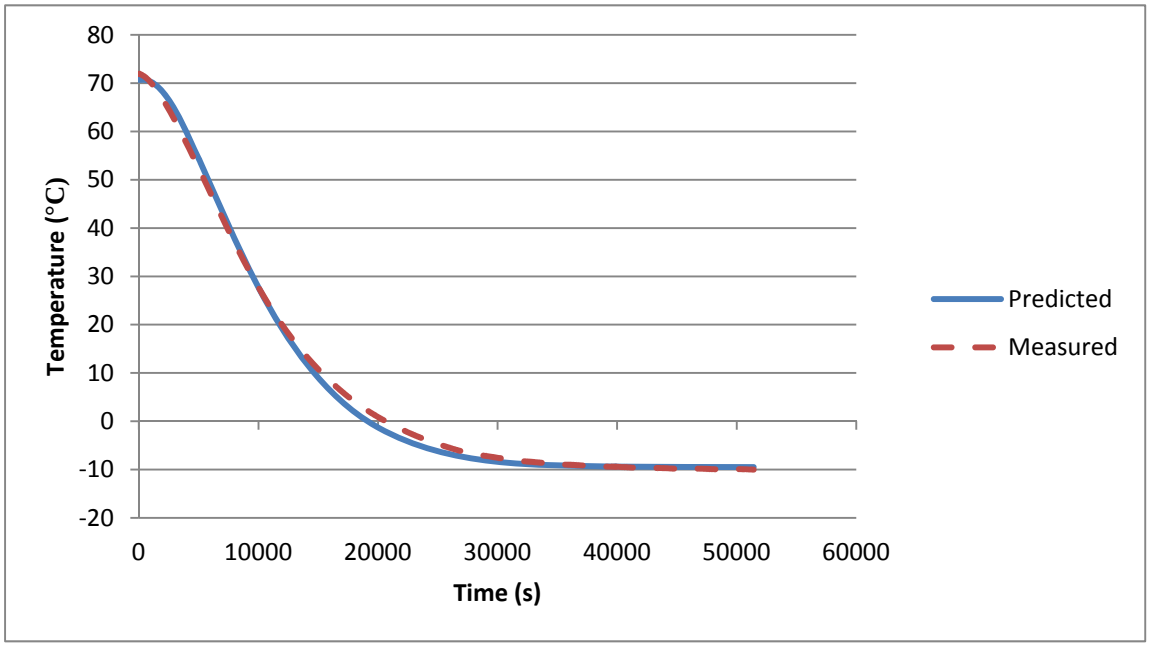

Figure 28 Front Wall of Shroud Decreasing Temperature Transient Results

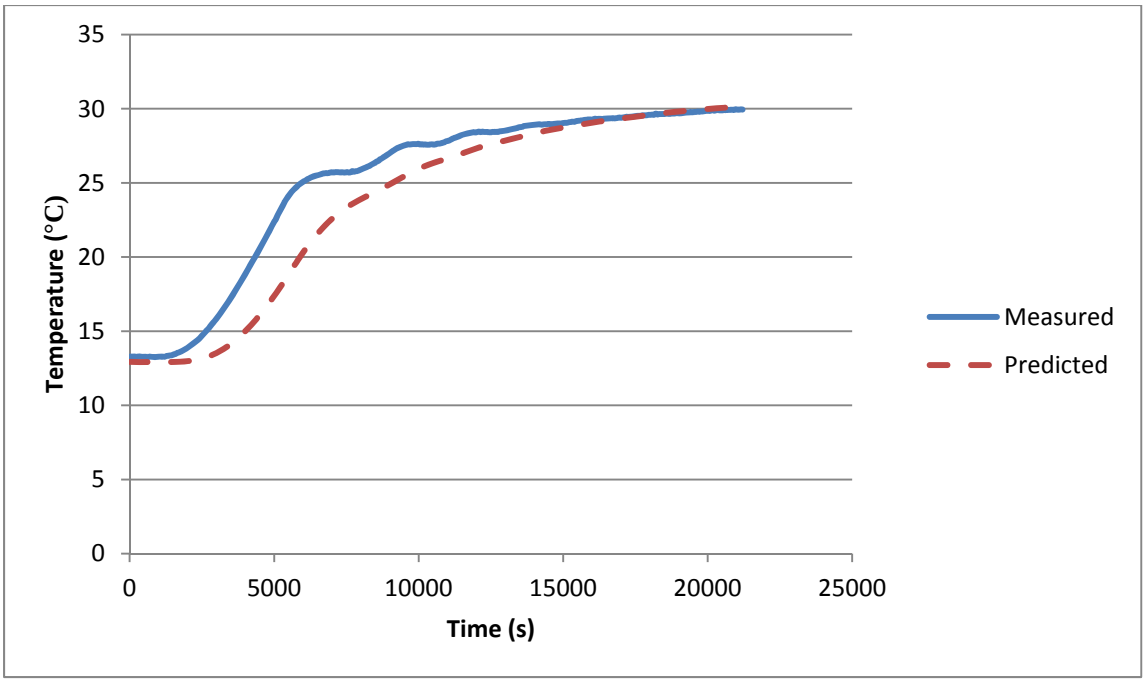

Figure 29 Quartz Window Increasing Temperature Transient Results

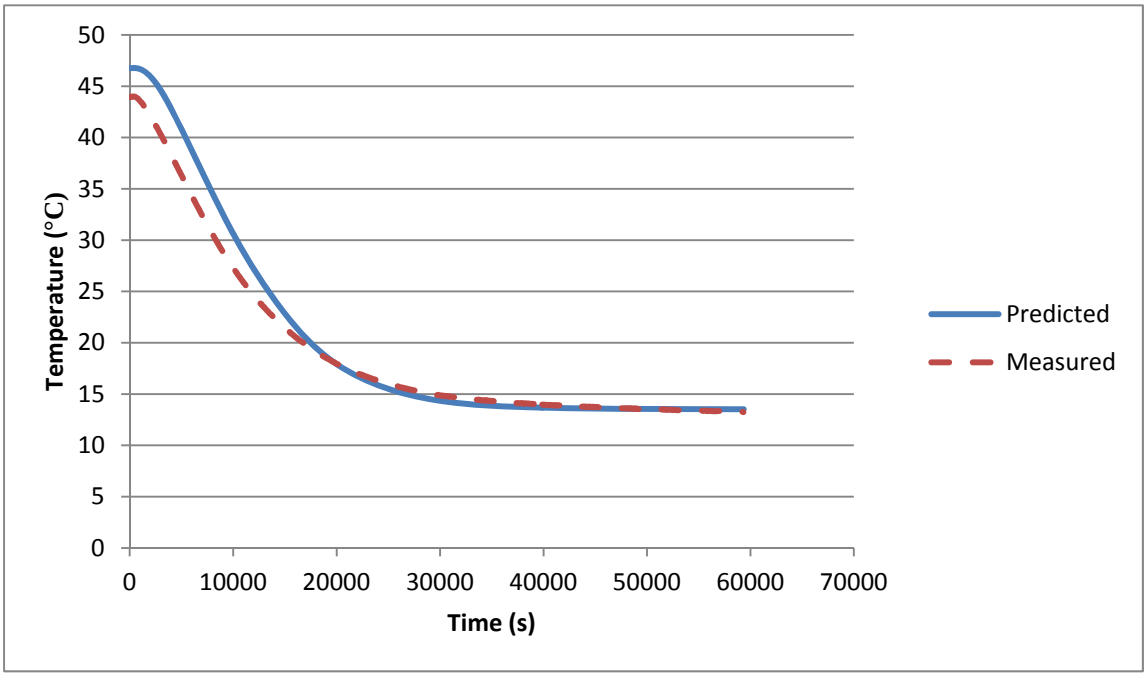

Figure 30 Quartz Window Decreasing Temperature Transient Results

Figures 31 and 32 show the transient computational predictions for the solar simulator flange as compared to the measured data with increasing and decreasing temperature respectively. The transient results for the solar simulator flange had an error of $T_{error} < 14.5°C$. Similar to the steady-state temperature predictions, the solar simulator flange computational predicted temperatures have the most significant error from measured values. This could potentially be attributed to the difference in geometry between the computational model and the actual flange. It is more likely this error is related to the modeling of the exterior environment affecting the flange. Specifically, the solar simulator flange is connected to the exterior wall of the chamber. The effects of this wall were not properly characterized to understand how its temperature relates to the flange and also the rear surface of the shroud wall, so this could be a large driver in the difference between predicted and measured solar simulator flange temperatures. Also, the solar gate valve is a large pneumatic valve that is integrated into the flange. Because of this, the gate valve also interacts with the solar simulator flange as well, which could cause effects not accurately captured within the model.

Although the TVAC environment computational model had significant error in predicting the temperature of the solar simulator flange, this is unlikely to cause significant error in test article temperature predictions within the overall TVAC environment, as mentioned in the steady-state results.

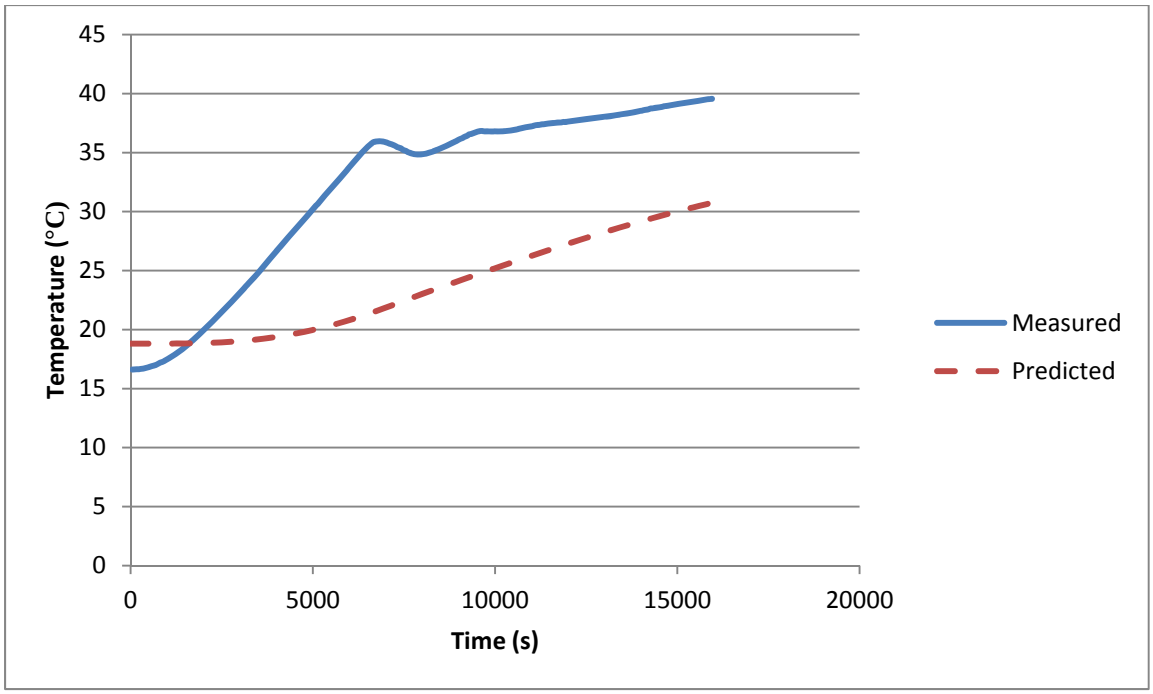

Figure 31 Solar Simulator Flange Increasing Temperature Transient Results

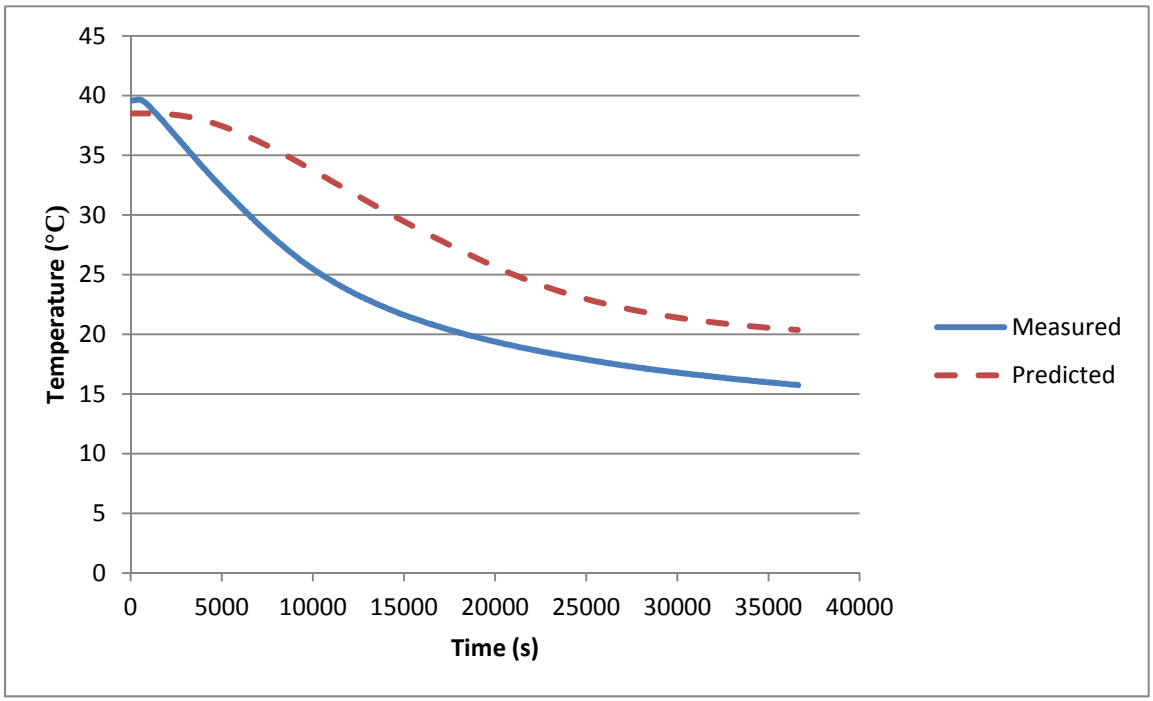

Figure 32 Solar Simulator Flange Decreasing Temperature Transient Results

Aluminum Plate Models

The 10x10 in. aluminum plate was tested with the general temperature profile with one exception. Due to other research test priorities, the test needed to be stopped prior to reaching the T = 10°C set point. Due to an unexpected error in a data log script, data was lost for the entire 6x6 in. aluminum plate test, and it was not rerun due to time constraints. The steady-state computational predictions and the measured results for the 10x10 in. aluminum plate are shown in Table 4.

Table 4 10x10 in. Aluminum Plate Steady-State Temperatures (°C)

Set Point	Predicted	Actual	T_{error}
T = -15 °C	-11.4	-10.9	0.5
T = 10 °C	11.3	Unknown	Unknown
T = 40 °C	39.3	40.3	1.0
T = 75 °C	72.3	72.7	0.4

The measured steady-state temperatures for the aluminum plate demonstrate a strong correlation to the predicted values from the computational model in the TVAC environment with a prediction error of $T_{error} < 1.0$°C. Figures 33 and 34 show the transient computational predictions for the 10x10 in. aluminum plate as compared to the measured data with increasing and decreasing temperature respectively. The transient results for the 10x10 in aluminum plate had an error of $T_{error} < 21.8$°C.

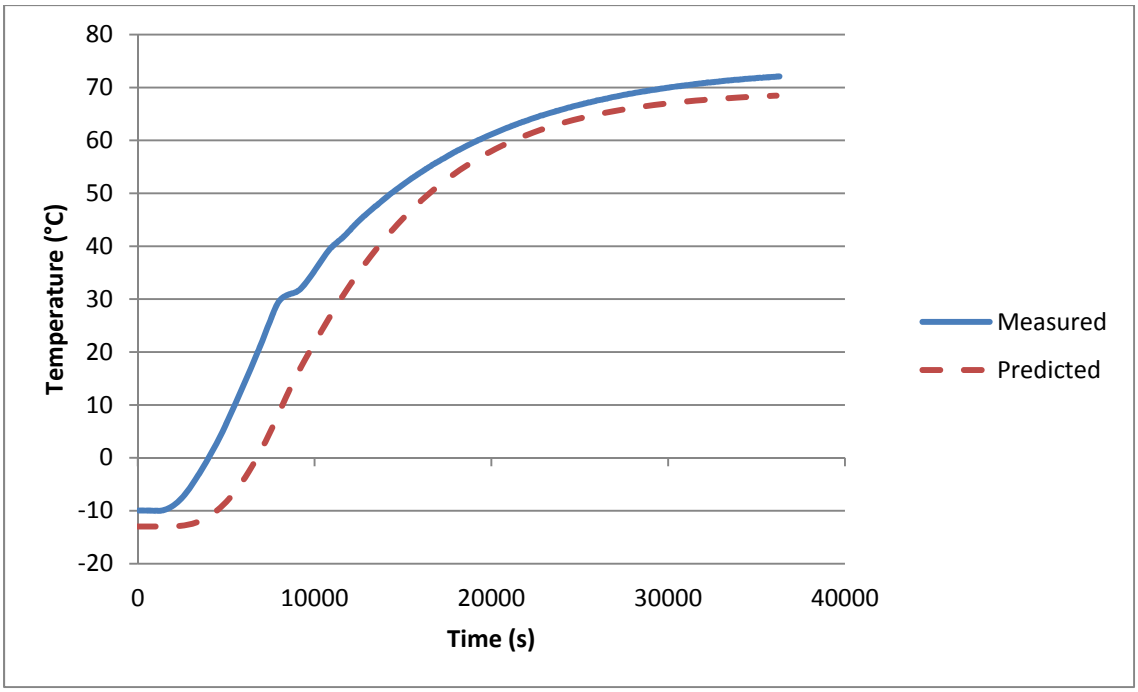

Figure 33 10x10 in. Aluminum Plate Increasing Temperature Transient Results

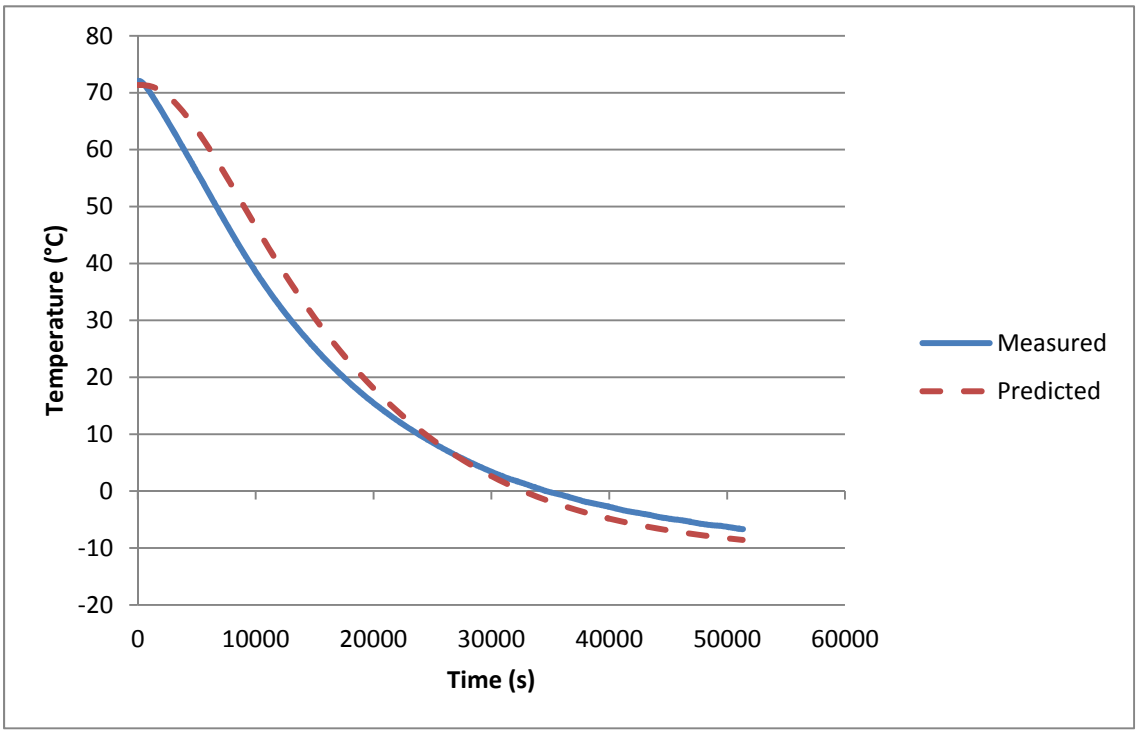

Figure 34 10x10 in. Aluminum Plate Decreasing Temperature Transient Results

The largest prediction error occurred during the increasing temperature case, which can be attributed to the faster ramp rates of the platen and shroud control temperatures when temperature is increasing rather than decreasing. With errors in the generated predictions, a faster ramp rate exacerbates these errors over time, instead of allowing the model to correct itself over time. The decreasing temperature case had prediction error of $T_{error} < 8.6°C$, which was still not accurate enough for validation but was a significant improvement on the increasing temperature predictions.

Similar to the quartz window transient predictions in Figure 29, the 10x10 in. aluminum plate increasing temperature predictions take a longer period of time than the measured values to start to change temperature. Once the aluminum plate prediction starts to change temperature, the slope of the change in temperature matches the slope of the measured data as shown in Figure 33. This means the time error could potentially be corrected for, which could provide a lower fidelity model validation capability to increase confidence in the transient predictions of the spacecraft thermal model.

It is unclear what could be causing this much transient prediction error within the model. While the solar simulator flange model had the most prediction error, including significant transient error, the solar simulator flange error should increase the aluminum plate's temperature change over time if it has any effect at all. This is because the predicted temperatures of the solar simulator flange were colder than measured temperatures when the chamber was hot and hotter than the measured temperatures when the chamber was cold as shown in Figures 31 and 32. This would cause the solar simulator flange in the computational model to emit more radiation when the chamber is cold or absorb more radiation when the chamber is hot as compared to the measured

environmental conditions. As previously stated, radiation of the solar simulator flange is also unlikely to have an appreciable effect on the temperature of the test article, due to the directionality of the flange surfaces.

The optical properties of the surfaces are also unlikely to be the cause of this prediction error. The optical properties of the chamber surfaces and the aluminum plate were varied within reasonable ranges (e.g. $\Delta\varepsilon = 0.1$ as compared to published values) in order to determine if this could increase the transient ramp rate of the aluminum plate predictions. Changes to the transient predictions were not significant enough to account for the prediction error and instead invalidated previous data correlation for the chamber itself.

What more likely causes these prediction errors is uncertainty in how Thermal Desktop® handles specular and diffuse reflection of surfaces. For this research, default parameters for the Monte Carlo/Ray Tracing algorithm within Thermal Desktop® were used in order to generate radiation predictions. Without errors in optical properties or the physical shape and temperature of the chamber within the computational model, the way radiation effects are calculated in the chamber is the only other likely source of error.

Summary

This chapter provided a summary of the results of the characterization experiments conducted in this research. Comparisons were also provided of the computational predictions and the measured data in order to determine the validity of the computational thermal model. Also, analysis was provided where unexpected behaviors were observed.

V. Conclusions and Recommendations

This chapter provides an overview of the conclusions and capabilities developed from this research. Specifically, the capabilities of the TVAC environment computational model and improved performance and understanding of the AFIT Solar Simulation TVAC are discussed. Lastly, recommendations for future work within this research area are provided.

Conclusions of Research

Since the TVAC environment and 10x10 in. aluminum plate predicted values demonstrated a strong steady-state correlation, the TVAC environment computational model is valid for use in steady-state temperature predictions for model validation. The ability to use the chamber for model validation and data correlation is a critical capability for spacecraft thermal analysis. This computational model could aid in mitigating the thermal risk of future CubeSat and payload programs.

Due to significant error in the transient predictions of the 10x10 in. aluminum plate, the TVAC environment computational model is not valid for use in transient temperature predictions for model validation. The TVAC environment computational model can provide a prediction of how the temperature of a test article should change over time, understanding that a time error in the computational predictions needs to be factored in.

Additionally, significant improvements to the performance and understanding of the AFIT Solar Simulation TVAC have been made throughout this research. Specifically, the chamber can now be upgraded and outfitted with specially coated copper plates in

order to better model on-orbit optical properties within the TVAC. This could be a critical asset in providing research sponsors with realistic and accurate testing of both CubeSats and payloads in the future.

Also, this research provides confidence in the procedures put in place to operate the solar simulator without concerns of damaging the Aeroglaze® coating on the incident wall of the shroud. This was critical as it was a significant unknown and a major concern when the TVAC was inspected for contract approval in August 2013.

Lastly, PID tuning reduced the steady-state error and the bounded oscillation of the platen and shroud controller temperatures to $|T_{fluc}| < 0.03$°C and $e_{ss} = 0.73$°C respectively. While the controllers are not optimized, these upgrades to controller performance significantly improve the TVAC's ability to achieve steady-state temperature set points for measurement of test article temperatures during testing. Without the ability to achieve a true steady-state temperature, the chamber would not be capable of providing accurate steady-state data for critical thermal balance and qualification testing.

Recommendations for Future Work

There are multiple ways to build upon the computational modeling of the AFIT Solar Simulation TVAC environment for future use. Since the TVAC was new and had some unknown capabilities, there were complications during the tests utilized in this research as mentioned previously. Since the data used to characterize the TVAC was incomplete in some cases and no repeatability testing was accomplished to verify measurements, more testing of the chamber through more profiles could complete this

data picture. Also, since there is significant transient error with the solar simulator flange and quartz window, further characterization and improvement of the models of these components of the chamber could be accomplished. Lastly, all experiments run for this research were accomplished with the solar simulator gate valve open. Closing this pneumatic valve will likely change the thermal environment and would therefore require a different model if tests were to be accomplished with it closed.

Also, a detailed analysis of the radiation calculations used within Thermal Desktop® could provide more confidence in how the software calculates radiation for transient solutions. While this research focused on modeling using the finite difference method, the finite element method could be explored instead. Any concerns with geometric fidelity could be mitigated by the complex geometries achievable with finite element modeling. This could potentially provide a solution to the errors in temperature on the solar simulator flange and the quartz window.

Additionally, time constraints prohibited this research from testing more articles within the chamber to provide greater validation. Most importantly, testing the additional aluminum plate to compare a test article with the exact same thermophysical and optical properties as the aluminum plate tested in this research would provide greater confidence in the TVAC environment model. Testing of actual spacecraft and payloads would also provide more opportunities as well to prove the utility of this computational model.

Although not necessary for basic data correlation, adding solar simulation to the TVAC environment model would provide a predictive tool for use when running any experiment, not just experiments without solar simulation. Also, without any visible light used during experiments, the absorptivity values of the surfaces of a test article are not

validated as a part of thermal balance testing. Computational modeling of solar simulation would provide this capability for the incident side of the spacecraft for a given test.

There are also ways in which the AFIT Solar Simulation TVAC itself can continue to be improved. As mentioned previously, the PID coefficients meet the objectives of this research but are still not optimized. More work could be done to ensure the PID coefficients are optimal for the use of the chamber. Similarly, temperature controllers with a larger bath size could improve the rise time, settling time, and low temperature capabilities of the TVAC. Additional insulation for the chamber could also improve the low temperature capabilities of the TVAC as well.

References

[1] Dunbar, B. and Mahoney, B., "CubeSat Launch Initiative," NASA, 18 November 2013. [Online]. Available: http://www.nasa.gov/directorates/heo/home/CubeSats_initiative.html. [Accessed 29 December 2013].

[2] Swartwout, M., "The First One Hundred CubeSats: A Statistical Look," *Journal of Small Satellites,* vol. 2, no. 2, 2014.

[3] Tilford, C. R., "Pressure and Vacuum Measurements," National Institute of Standards and Technologies, 1992. [Online]. Available: http://www.nist.gov/calibrations/upload/pmc-2.pdf. [Accessed 07 March 2014].

[4] Smith, K. D., *Environmental Testing and Thermal Analysis of the NPS Solar Cell Array Tester*, MS thesis, Naval Postragraduate School, Monterey, June 2011.

[5] FIncropera, F. P., DeWitt, D. P., Bergman, T. L., and Lavine, A. S., *Fundamentals of Heat and Mass Transfer*, Hoboken: John Wiley & Sons, Inc., 2007.

[6] Siegel, R. and Howell, J. R., *Thermal Radiation Heat Transfer*, Washington D.C.: Taylor & Francis, 1992.

[7] Planck, M., *The Theory of Heat Radiation*, New York: Dover Publications, 1959.

[8] Gilmore, D. G., *Spacecraft Thermal Control Handbook Volume I: Fundamental Technologies*, El Segundo: The Aerospace Press, 2002.

[9] Anderson, B., Justus, C. and Batts, W., *Guidelines for the Selection of Near-Earth Thermal Environment Parameters for Spacecraft Design*. NASA Technical Memorandum TM-2001-211221. Huntsville: NASA MSFC, 2001.

[10] Wertz, J. R., Everett, D. F., and Puschell, J. J., *Space Mission Engineering: The New SMAD*, Hawthorne: Microprism Press and Springer, 2011.

[11] NASA Goddard Space Flight Center, *General Environmental Verification Standard.* GSFC-STD-7000A. Greenbelt: NASA Goddard, 2013.

[12] University of Michigan, "Introduction: PID Controller Design," 2012. [Online]. Available: http://ctms.engin.umich.edu/CTMS/index.php?example=Introduction&section=ControlPID#1. [Accessed 02 02 2014].

[13] Samson, S., Choueiry, E., and Pang, K, "Thermal Balance Testing of the MSAT Spacecraft", *Space Simulation Conference on Space Mission Success Through Testing, 18th*, Baltimore, 1994.

[14] Jin, Z., Joshi, S. C., Nesamani, G. J. J., Chan, P. K., Ying, T. M., and Goh, C. H., "Data Analysis and Correlation for Thermal Balance Test on a Micro-Satellite Model," *Heat Transfer Engineering,* vol. 31, no. 3, pp. 222-233, 2010.

[15] Richmond, J. A., *Adaptive Thermal Modeling Architecture for Small Satellite*, MS thesis, SSL-#4-10, Massachusetts Institute of Technology, Cambridge, 2010.

[16] Urban, D. A., *Application of Commercial Software to CubeSat Thermal Analysis.* MS thesis, AFIT/GA/ENY/12-M41, School of Engineering and Management, Air Force Institute of Technology, Wright-Patterson AFB OH, March 2012.

[17] Panczak, T. D., Ring, S. G., Welch, M. J., Johnson, D., Cullimore, B. A., and Bell, D. P., "Thermal Desktop User's Manual," Cullimore & Ring Technologies, Boulder, 2013.

[18] Ball Aerospace & Technologies Corp., "Space Test Program - Standard Interface Vehicle Payload User's Guide," Ball Aerospace & Technologies Corp., Boulder, 2013.

[19] Perry, D., *Space Object Self-Tracker Hardware Analysis and Environmental Testing.* MS Thesis, AFIT-ENY-14-M-39, School of Engineering and Management, Air Force Institute of Technology, Wright-Patterson AFB OH, March 2014.

[20] Bell, D. P., Panczak, T. D., and Cullimore, B. A., "Thermal Desktop Advanced Modeling Guide", Cullimore and Ring Technologies, Boulder, 2013.

Vita

Captain Daniel M. Hatzung grew up in St. Paul, Minnesota. He entered undergraduate studies at the University of Minnesota in Minneapolis, Minnesota where he graduated with a Bachelor of Science degree in Mechanical Engineering in May 2009. He was commissioned through AFROTC Detachment 415 at the University of Minnesota.

His first assignment was at Edwards AFB in July 2009 where he was the Global Observer Project Lead for the 452nd Flight Test Squadron and then Executive Officer for the 412th Operations Group. In August 2012, he entered the Graduate School of Engineering and Management, Air Force Institute of Technology in pursuit of a Master of Science in Astronautical Engineering. Upon graduation, he will be assigned to the Air Force Research Laboratory Aerospace Systems Directorate.

REPORT DOCUMENTATION PAGE

Form *Approved*
OMB No. 0704–0188

1. REPORT DATE (DD–MM–YYYY)	2. REPORT TYPE	3. DATES COVERED *(From — To)*
17-03-2014	Master's Thesis	September 2012-March 2014

4. TITLE AND SUBTITLE
Thermal Characterization of the Air Force Institute of Technology Solar Simulation Thermal Vacuum Chamber

5a. CONTRACT NUMBER
5b. GRANT NUMBER
5c. PROGRAM ELEMENT NUMBER

6. AUTHOR(S)
Hatzung, Daniel, M., Capt

5d. PROJECT NUMBER
5e. TASK NUMBER
5f. WORK UNIT NUMBER

7. PERFORMING ORGANIZATION NAME(S) AND ADDRESS(ES)
Air Force Institute of Technology
Graduate School of Engineering and Management (AFIT/EN)
2950 Hobson Way
Wright-Patterson AFB OH 45433-7765

8. PERFORMING ORGANIZATION REPORT NUMBER
AFIT-ENY-14-M-23

9. SPONSORING / MONITORING AGENCY NAME(S) AND ADDRESS(ES)
Capt Shuck, Timothy J.
Guidance, Navigation, & Control Analyst
AFRL/RVES
3550 Aberdeen SE, Bldg 497
Kirtland AFB, NM 87117
COMM (505) 853-4513 DSN 263-4513

10. SPONSOR/MONITOR'S ACRONYM(S)
AFRL/RV

11. SPONSOR/MONITOR'S REPORT NUMBER(S)

12. DISTRIBUTION / AVAILABILITY STATEMENT
Distribution Statement A. Approved for Public Release; Distribution Unlimited

13. SUPPLEMENTARY NOTES
This work is declared a work of the U.S. Government and is not subject to copyright protection in the United States.

14. ABSTRACT

Although predictive thermal modeling on CubeSats has previously been accomplished, a method to validate these predictive models with terrestrial experiments is essential for developing confidence in the model. As a part of this effort, AFIT has acquired a new Solar Simulation Thermal Vacuum Chamber. This research analyzed the thermal environment to which a test article is exposed within the AFIT Solar Simulation Thermal Vacuum Chamber. A computational model of the thermal environment in the chamber was created and then validated using an experimental buildup approach through thermal balance testing of the empty chamber and an aluminum plate. First, the modeled surface temperatures of the thermal vacuum chamber interior walls were validated within Terror < 4°C of steady-state experimental data. Next, the aluminum plate computational model was validated within Terror < 1°C of steady-state experimental data. Through these results, this research provides the capability to validate spacecraft and payload computational thermal models within the thermal vacuum chamber environment by comparing computational predictions to experimental data for steady-state cases. Additionally, this research validated an upgrade to increase optical performance of the TVAC by bolting a copper plate coated with Aeroglaze® black paint to the top of the platen, ensured safe procedures are in place for solar simulation, and improved the temperature controller performance.

15. SUBJECT TERMS
Heat Transfer, Thermal Vacuum Chamber, Space Qualification, Thermal Balance Test, Radiation, Conduction, Thermal Model, CubeSat, Solar Simulation

16. SECURITY CLASSIFICATION OF:			17. LIMITATION OF ABSTRACT	18. NUMBER OF PAGES	19a. NAME OF RESPONSIBLE PERSON
a. REPORT	b. ABSTRACT	c. THIS PAGE			James L. Rutledge, Maj, USAF, AFIT/ENY
U	U	U	UU	94	19b. TELEPHONE NUMBER (Include Area Code) (937) 255-6565, x 4734 (james.rutledge@afit.edu)

Standard Form 298 (Rev. 8–98)
Prescribed by ANSI Std. Z39.18